NACA RM L53A02

RESEARCH MEMORANDUM

A THEORETICAL ANALYSIS OF THE DISTORTION OF FUEL-SPRAY-PARTICLE PATHS IN A HELICOPTER RAM-JET ENGINE DUE TO CENTRIFUGAL EFFECTS

By S. Katzoff and Samuel L. Smith, III

Langley Aeronautical Laboratory
Langley Field, Va.

NATIONAL ADVISORY COMMITTEE FOR AERONAUTICS

WASHINGTON

April 7, 1953
Declassified December 7, 1953

NATIONAL ADVISORY COMMITTEE FOR AERONAUTICS

RESEARCH MEMORANDUM

A THEORETICAL ANALYSIS OF THE DISTORTION OF FUEL-SPRAY-PARTICLE PATHS IN A HELICOPTER RAM-JET ENGINE DUE TO CENTRIFUGAL EFFECTS

By S. Katzoff and Samuel L. Smith, III

SUMMARY

Certain anomalies in the behavior of a ram-jet engine tip-mounted on a rotating helicopter blade had led to the suggestion that centrifugal effects were distorting the fuel-spray pattern. The present paper is a theoretical study of these effects. The differential equations of motion of the spray particles were set up and integrated numerically for sixty-four selected combinations of the various parameters. For greater ease of computation, all but one of these cases were confined to two-dimensional motion of the particles (that is, motion in the plane of the rotor). A simple method for determining the approximate final direction of travel of the particles, without solving the equations of motion, was developed.

Plots of the solutions show that centrifugal action does have a marked effect in deflecting the larger particles toward the outer wall (that is, the wall of the combustion chamber that is farthest from the center of the rotor) and thus out of the main combustion region. Reduction of the particle size alone probably would not solve the problem, since the fine particles may not move far enough laterally from the nozzle before being carried downstream in a rich-mixture cylindrical core near the center of the combustion chamber. Several suggestions for alleviating the fuel-distribution problem are given.

INTRODUCTION

In some recent experimental studies of a ram-jet engine mounted on the tip of a helicopter blade, it appeared that the thrust obtained was less than that measured in bench tests of the same engine in an air stream

of velocity equal to the rotor tip speed; also, the combustion was more erratic. One suggested explanation of the difference is that the fuel particles are thrown radially outward by centrifugal action, with resulting asymmetric fuel distribution and accumulation of fuel toward the outer wall (that is, the wall of the combustion chamber that is farthest from the center of the rotor). Contour-like stains on the outer wall of the jet unit, presumably caused by a pool of liquid fuel, served to substantiate this theory.

The present analysis was undertaken to determine the plausibility of this theory, to determine the range of fuel particle sizes for which such an effect would be appreciable, and to learn the relative importance of some of the other parameters involved. Essentially, the analysis consists in setting up the differential equations of motion of the fuel droplets in a rotating flow field and integrating for several values of some of the major parameters. The air flow in the ram jet was assumed to be nonturbulent and moving along circular streamlines with uniform angular velocity about the center of the rotor. Because of these and other idealizations, the results, which are presented as plots of fuel-particle paths, cannot be considered as quantitative representations of actual paths; the results do, however, define the range of parameters within which centrifugal effects become important.

For further simplification of the computations, the majority of the cases considered were confined to two-dimensional motion of the fuel particles; that is, motion in a plane perpendicular to the axis of rotation. Sixty-three two-dimensional cases were calculated, corresponding to selected combinations of three particle sizes, two rotor radii, two angular velocities, two internal-flow velocities, two fuel injection velocities, and three fuel injection angles (all in the upstream direction). One three-dimensional case, corresponding to injection of the fuel particle out of the plane of rotation of the nozzle, was calculated to give a general indication of the effect of a third (normal) component of the initial velocity on the particle path.

SYMBOLS

x, y, z rectangular coordinates in fixed reference frame; origin at center of rotor (see fig. 1)

r, θ, z cylindrical coordinates, relative to reference frame rotating about z-axis at center of the rotor (see fig. 1)

r, ψ, z coordinates of the fuel particles in a rotating reference frame moving with the fuel nozzle (see fig. 1)

ω angular velocity of rotation of the r, θ, z system with respect to the x, y, z system

σ angular velocity of rotation of the spray nozzle relative to the r, θ, z system

ρ_a air density

ρ_f fuel density

ν kinematic viscosity of air

D diameter of spherical fuel particle

R Reynolds number of fuel particle

C_D drag coefficient of fuel particle

β initial injection angle of fuel particle, measured with respect to the forward direction (normal to radius), positive outboard

t time

m mass of the fuel particle

g acceleration of gravity

Subscripts:

o indicates initial value (at the time of ejection)

ANALYSIS

Assumptions.- The analysis was made on the basis of the following simplifying assumptions:

(1) The fuel particles are spherical, so that available data for the drag coefficient of a sphere may be used

(2) Evaporation of the droplets is negligible; that is, the radius of the droplet is constant

(3) The effect of gravitational force on the particles is negligible

(4) The air flowing over the fuel spray is without turbulence and has a constant velocity with respect to the nozzle

The first three assumptions are considered to be satisfactorily valid over the region of travel of the fuel particles prior to burning. The fourth assumption is much more arbitrary but is considered satisfactory for the present purpose.

Sphere drag.- It is necessary to determine the drag of a sphere as a function of size and velocity in order to set up and solve the equations of motion of the fuel particles. A considerable simplification of the equations of motion would have resulted had it been permissible to use Stokes' classical law of drag of a sphere (because of the simple proportionality between drag and velocity). Unfortunately, however, the Reynolds numbers encountered ($20 < R < 1000$) extend well beyond the range for which Stokes' law or any of its several modifications is valid, and empirical data, such as that given in references 1, 2, and 3, had to be used. The empirical curve of drag coefficient against Reynolds number from reference 1 is shown as a dotted line for this range in figure 2. Since the equations of motion were to be solved numerically on the Bell Telephone Laboratories X-66744 relay computer at the Langley Laboratory, an algebraic expression for the drag was required. The empirical drag curve was approximated in the desired interval by the equation

$$C_D = \frac{72.56}{R + 13.04} + 0.415 \tag{1}$$

for purposes of computation. The curve of this equation is also shown in figure 2. Its maximum error in the range $20 < R < 1000$ is about 5 percent and its mean error is less than 3 percent. Actually the initial Reynolds numbers for a few cases were somewhat above 1000, but the resulting error was small, that is, well within the accuracy of the analysis.

The velocity that produces drag is, of course, the particle velocity relative to the local (internal) air. In the following analysis the three mutually perpendicular components of this relative velocity are $\dot{r}$, $r\dot{\theta}$, and $\dot{z}$. Therefore, the resultant relative velocity will be $\sqrt{\dot{r}^2 + r^2\dot{\theta}^2 + \dot{z}^2}$, which, together with the particle size and the kinematic viscosity of the air, determines the Reynolds number and hence the drag coefficient. The net drag, which is directed so as to oppose the relative motion of the particle, is given by

$$\text{Drag} = \frac{\rho_a}{2} \frac{\pi D^2}{4} C_D\left(\dot{r}^2 + r^2\dot{\theta}^2 + \dot{z}^2\right) \tag{2}$$

and the three mutually perpendicular components of the drag are given by

$$(\text{Drag})_r = \frac{\rho_a}{2} \frac{\pi D^2}{4} C_D \dot{r}\sqrt{\dot{r}^2 + r^2\dot{\theta}^2 + \dot{z}^2} \tag{2a}$$

$$(\text{Drag})_\theta = \frac{\rho_a}{2} \frac{\pi D^2}{4} C_D r\dot{\theta}\sqrt{\dot{r}^2 + r^2\dot{\theta}^2 + \dot{z}^2} \tag{2b}$$

$$(\text{Drag})_z = \frac{\rho_a}{2} \frac{\pi D^2}{4} C_D \dot{z}\sqrt{\dot{r}^2 + r^2\dot{\theta}^2 + \dot{z}^2} \tag{2c}$$

Differential equations of motion of spray particles.- For convenience the motion of the spray particles will be considered relative to a reference frame rotating with an angular velocity equal to the angular velocity of the internal air in the ram-jet unit. For example, for a ram-jet unit operating at a tangential velocity (tip speed) of 800 fps with respect to air at rest and an internal air-flow velocity of 200 fps relative to the nozzle and walls, the internal air has an absolute velocity (with respect to a fixed reference frame) of 600 fps, so that the angular velocity of the rotating reference frame has the value $\omega = \frac{600}{r_o}$ radians per second, where r_o is the radial distance to the center of the fuel nozzle; therefore, in the general case, $\omega = \frac{\text{Tip speed - Internal-flow velocity}}{\text{Initial radius}}$. The choice of this rotating reference frame presents some computational advantage, since the velocity of the particle relative to this system is the velocity that produces drag. Furthermore, since these drag forces tend to constrain the particle to move with this flow, it is this value of ω that determines the eventual centrifugal acceleration of the particle.

In this rotating reference frame, let the particle coordinates be r, θ, and z so that, relative to a stationary reference frame (x, y, z), the coordinates are r, $\theta + \omega t$, and z, where t is time elapsed since these two frames coincided. The following relations, therefore, connect the rotating cylindrical and stationary rectangular systems:

$$x = r \cos(\theta + \omega t)$$

$$y = r \sin (\theta + \omega t)$$

$$z = z$$

Differentiating twice to obtain the acceleration gives:

$$\ddot{x} = \ddot{r}\cos(\theta + \omega t) - 2\dot{r}(\dot{\theta} + \omega)\sin(\theta + \omega t) - r(\dot{\theta} + \omega)^2\cos(\theta + \omega t) - r\ddot{\theta}\sin(\theta + \omega t)$$

$$\ddot{y} = \ddot{r}\sin(\theta + \omega t) + 2\dot{r}(\dot{\theta} + \omega)\cos(\theta + \omega t) - r(\dot{\theta} + \omega)^2\sin(\theta + \omega t) + r\ddot{\theta}\cos(\theta + \omega t)$$

$$\ddot{z} = \ddot{z}$$

In order to find the radial and tangential components of the acceleration at time t, assume that at that instant the radius coincides with the x-axis, so that $\ddot{x}$ and $\ddot{y}$ will be the two desired components. At this instant $(\theta + \omega t)$ is zero and the equations reduce to

$$\ddot{x} = \ddot{r} - r(\dot{\theta} + \omega)^2$$

$$\ddot{y} = r\ddot{\theta} + 2\dot{r}(\dot{\theta} + \omega)$$

$$\ddot{z} = \ddot{z}$$

Thus, the radial acceleration consists of $\ddot{r}$ plus the centrifugal acceleration, and the tangential acceleration consists of $r\ddot{\theta}$ plus the Coriolis acceleration. These three acceleration components are now related (since force = mass × acceleration) to the previously derived drag components (eqs. (2a), (2b), and (2c)) to give the following equations:

$$-\frac{\rho_a}{2m}\left(\frac{\pi D^2}{4}\right)C_D\,\dot{r}\sqrt{\dot{r}^2 + r^2\dot{\theta}^2 + \dot{z}^2} = \ddot{r} - r(\dot{\theta} + \omega)^2$$

$$-\frac{\rho_a}{2m}\left(\frac{\pi D^2}{4}\right)C_D\,r\dot{\theta}\sqrt{\dot{r}^2 + r^2\dot{\theta}^2 + \dot{z}^2} = r\ddot{\theta} + 2\dot{r}(\dot{\theta} + \omega)$$

$$-\frac{\rho_a}{2m}\left(\frac{\pi D^2}{4}\right)C_D\,\dot{z}\sqrt{\dot{r}^2 + r^2\dot{\theta}^2 + \dot{z}^2} = \ddot{z}$$

where

$$C_D = \frac{72.56}{R + 13.04} + 0.415$$

and where the mass of the particle m is expressed as

$$m = \frac{\pi D^3 \rho_f}{6}$$

Substituting for m and rearranging gives:

$$\ddot{r} + \frac{3\rho_a}{4\rho_f D} C_D \dot{r}\sqrt{\dot{r}^2 + r^2\dot{\theta}^2 + \dot{z}^2} - r(\dot{\theta} + \omega)^2 = 0 \qquad (3a)$$

$$r\ddot{\theta} + \frac{3\rho_a}{4\rho_f D} C_D r\dot{\theta}\sqrt{\dot{r}^2 + r^2\dot{\theta}^2 + \dot{z}^2} + 2\dot{r}(\dot{\theta} + \omega) = 0 \qquad (3b)$$

$$\ddot{z} + \frac{3\rho_a}{4\rho_f D} C_D \dot{z}\sqrt{\dot{r}^2 + r^2\dot{\theta}^2 + \dot{z}^2} = 0 \qquad (3c)$$

These three equations constitute the system of differential equations that must be solved in order to obtain the paths of the particles. For the cases of two-dimensional motion of the particle (z constant), equation (3c) is eliminated and the term $\dot{z}^2$ is dropped from the remaining two equations.

Solution of equations.- As was mentioned previously, most of the calculations were performed on the Bell relay computer. The process was essentially a step-by-step numerical integration of the simultaneous equations (3a) and (3b) by Heun's method (ref. 4). For the calculation of any particular case, ω is given, as previously described, by the rotor tip speed, the internal airspeed relative to the walls of the jet unit, and the radius r_o from the rotor axis to the fuel nozzle. The assumed outward and upward components of the fuel-injection velocity relative to the nozzle give the initial values of $\dot{r}$ and $\dot{z}$. If the forward injection-velocity component relative to the nozzle is given by, say, v_t, then the total tangential velocity of the particle relative

to the fixed frame is the tip speed + v_t, which must be the initial value of $(\omega + \dot{\theta})r_o$. That is, initially

$$\text{Tip speed} + v_t = (\omega + \dot{\theta}_o)r_o$$

Thus

$$\dot{\theta}_o = \frac{(\text{Tip speed} - \omega r_o) + v_t}{r_o}$$

or

$$\dot{\theta}_o = \frac{\text{Internal flow speed (relative to wall)} + v_t}{r_o}$$

The initial values of θ and z may be taken as zero. For each path the selected initial conditions were specified and a suitable interval for the integration steps was chosen. In all the two-dimensional cases, time increments of 0.0004 second were used for the early parts of the paths, and increments of 0.0008 second were used after the particle had approximately established its final direction. The one three-dimensional calculation was performed manually by Euler's method (ref. 4), with 0.0002-second time increments for the early parts and 0.0004-second increments for the later parts of the path.

These calculations give the particle paths in the original rotating coordinate system (r, θ, z). Before plotting the particle paths, however, it was considered desirable to transform to a system moving with the ram jet itself, so that the curves would show the paths as they would appear to an observer riding on the ram-jet nozzle. This transformation may be easily performed by shifting the angular displacement of each point of the path by σt, where σ is the angular velocity of the ram jet relative to that of the internal air in the ram jet, and t is the time required for the particle to travel to that point from the injection nozzle. This new angular location is that given in figures 3 to 19 and is designated by ψ, where ψ is related to θ by the equation

$$\psi = \theta - \sigma t$$

RESULTS

Cases calculated.- The values of the parameters and initial conditions used to calculate the sixty-three two-dimensional cases considered

in the present report are presented in table I. The first thirty-six cases listed in this table are all possible combinations of three particle sizes, three injection angles, two rotor radii, two tip speeds, one injection velocity, and one internal-flow speed. The remaining twenty-seven cases were considered to ascertain the effect of increasing the internal-flow velocity or the fuel injection velocity or both. The centrifugal accelerations at the fuel nozzle for the cases calculated are 1330g for r_o = 15 feet and 800 fps tip speed, 795g for r_o = 25 feet and 800 fps tip speed, 2070g for r_o = 15 feet and 1000 fps tip speed, and 1240g for r_o = 25 feet and 1000 fps tip speed. The cases covered are considered to be fairly representative of the region of present interest and to define the limits of the problem.

The fuel density was constant at 1.61 slugs/cu ft throughout all the calculations. The values of the air constants used were: air density, 0.00238 slug/cu ft; and air kinematic viscosity, 0.000172 ft^2/sec. These values of the air characteristics correspond to operation at altitudes of about 4000 feet for the 800 fps tip speed, and 9000 feet for the 1000 fps tip speed. These altitudes are only approximate since they depend on inlet losses and atmospheric conditions.

The values for the case of three-dimensional motion are: particle size D = 0.004 inch; rotor radius r_o = 25 feet; tip speed, 800 fps; internal-air velocity with respect to the nozzle, 200 fps; fuel-injection velocity relative to the nozzle, 150 fps; injection direction, in the vertical plane through the ram-jet axis normal to the radius ($\beta = 0^o$) but inclined 45^o from the plane of the rotor.

Results of the calculations.- Figures 3 to 18 present the particle paths for the sixty-three two-dimensional cases that were calculated, and figure 19 presents the particle path for the three-dimensional case. It should be noted that the curve corresponding to $\beta = 0^o$, D = 0.004 inch, is given on both figures 7 and 8 for ease of comparison. This repetition also occurs on figures 11 and 12 and on figures 15 and 16. The outline of the walls and flame holders of the particular ram-jet unit that occasioned this investigation is dotted in on figure 3(a). It will be noted that the plotted paths extend well into the combustion chamber. Actually, these later portions of the paths can not be considered generally valid, because of combustion, turbulence and other effects; also, many particles may be caught on the flame holders. These portions are shown here, however, not only for the sake of completeness, but also because they might be applicable for larger ram-jet units, with greater distance between the nozzles and the flame holders.

The calculated points are shown on the paths in order to indicate the time history of the particles and to provide means for estimating velocities and accelerations. For the two-dimensional cases the points

represent time intervals of 0.0004 second over the first, highly curved, parts of the path, and 0.0008 second over the later, nearly straight parts. The point where the interval is doubled is easily identifiable on each path. Similarly, the projection lines in the three-dimensional plot of figure 19 indicate time intervals of 0.0002 second for the initial portion of the curve and 0.0004 second for the later portions.

DISCUSSION

Particle-path distortion.- All the curves (figs. 3 to 19) show similar characteristics. There is an initial sharply curved part, in which the general direction of travel changes from forward to rearward, followed by the approach to a fairly well-defined final direction. The distortion of the particle paths due to centrifugal force is clearly evident on all the curves. The centrifugal forces effectively superimpose an outward motion to the particles, so that the curves are deviated from the center and have an outwardly inclined final direction. Increased tip speed and decreased rotor radius, both of which result in increased centrifugal effects, are accompanied by increased displacement and inclination of the path. In this connection, a comparison of the curves of figure 3 with the corresponding curves of figure 6 reveals that the paths are nearly identical, especially for the smaller particles; a simple calculation shows that the centrifugal acceleration ($\omega^2 r$) is almost the same for both cases, even though the radii and tip speeds are quite different. Increased internal-flow velocity (compare, for example, fig. 11 with fig. 4(b)) results in less centrifugal distortion since the particles are turned and carried downstream more rapidly; thus, the centrifugal forces have less time in which to act. Increasing particle size has the opposite effect (see, for example, fig. 8) - since the mass (and hence $m\omega^2 r$) increases much more rapidly with particle diameter than does the air drag, the centrifugal distortion is accentuated.

With the lower internal air speed, only the paths of the smallest particles undergo deviations sufficiently small to appear reasonably acceptable. These smallest particles, however, do not penetrate very far outward before they are turned downstream (see fig. 3(a) or 5(a)), so that use of a very fine spray may result merely in a narrow column of very rich mixture passing through the combustion chamber. Increased ejection velocity of the fine particles somewhat increases the width of the column and thereby helps alleviate the problem; however, the use of several fine-spray nozzles distributed across the duct area ahead of the combustion chamber is probably the most direct solution. Increasing both the particle size and the internal air speed (figs. 15 to 18) also results in a broader column without excessive outward inclination of the paths; these higher internal air speeds are, however, probably too high for stable burning.

Although the present results clearly indicate the nature of the problem imposed by the centrifugal effects, it is apparent that the analysis was considerably idealized; and some judgment, based on an understanding of the nozzle spray characteristics (particle size and velocity distribution) and of the flow within the ram jet, would be required in applying the present results in the development of a helicopter ram jet. For example, the internal-flow velocity is not uniform, as has been here assumed, but is high in the inlet just ahead of the nozzles, decreases as it passes down the diffuser to the combustion chamber, and then increases again as combustion proceeds along the chamber. In addition there is a low-velocity stagnation region immediately ahead of the nozzle and its attachment brackets, so that the outward penetration of the particles immediately after ejection may be much more than here shown; this effect would result in increasing the width of the fuel spray column that passes into the combustion chamber. Furthermore, instead of all particles being ejected from one point, as assumed in the present calculations, there is frequently a cluster of nozzles, the spread of which adds to the width of the fuel spray column. Finally, it should be pointed out that the implied assumption of a smooth laminar type of flow past the nozzles and through the combustion chamber is considerably at variance with the actual state of the flow. The large-scale turbulence produced by the flame holders will serve to broaden the distribution of the spray particles. The distribution of the finest particles will be broadened considerably beyond that indicated in, say, figure 3(a) and the turbulence may even suffice to prevent some or most of the intermediate particles from being thrown directly to the outer wall by the centrifugal effects. It seems doubtful, however, that the turbulence could similarly keep an appreciable proportion of the larger particles from being thrown to the wall. In this connection an additional effect should be noted. Because the centrifugal acceleration of the air within the ram jet may be of the order of 500 to 1000g, the radial pressure gradient within the ram jet may correspondingly be 500 to 1000 times the vertical pressure gradient of the atmosphere. Rough calculations show that, in such pressure gradients, the air-density variations resulting from burning can result in convection currents comparable in violence to the turbulence introduced by the flame holders.

With regard to general methods of alleviating the problem presented by centrifugal effects, the use of fine-spray nozzles, high ejection speeds, and distributed arrangment of the nozzles have already been indicated. Ejecting most of the fuel inward and grouping the nozzles inboard of the ram-jet axis should also be helpful. Another possibility is skewing the inlet and combustion chamber so that the walls would be more nearly parallel to the skewed (or outwardly inclined) particle paths. Theoretically, there need be no corresponding loss in thrust for such a design as long as the exit direction remains normal to the rotor blade; however, the external drag of such a configuration may be excessive. In any case it seems likely that an adequate solution may be obtained for any given design problem by following these or similar approaches.

Limiting direction of particle paths.- It is interesting to note that the later portions of the three fuel particle paths corresponding to the three injection angles appear to be approximately parallel; that is, their directions are approximately independent of the initial injection angle. Since this direction is fairly indicative of whether the particle will pass into the combustion zone or be lost on the outer wall, an effort was made to develop a simple method for approximating this direction without actually going through a solution of the differential equations. Such a method would be useful for a rough evaluation of the path for cases that are not within the range covered in figures 3 to 18 of the present report.

In a strict sense, a "final" direction may not be clearly definable - the particle path (relative to the nozzle) probably approached some spiral asymptote, the exact shape of which is somewhat irregular owing, for example, to the variation of Reynolds number along the path. In any case, the present problem is not concerned with the final direction when r approaches infinity, but rather with the direction when r is of the order of r_o (or perhaps a few inches more than r_o, as indicated on the curves of figures 3 to 18) and the path curvature has decreased practically to zero. Specifically, it is proposed to put the second derivatives equal to zero in the differential equations (eqs. (3a) and (3b)), put r equal to r_o (or perhaps a few inches more than r_o), and solve the two equations algebraically for $\dot{r}$ and $\dot{\theta}$, which, together with r, determine the direction of the particle.

Letting $\ddot{r} = \ddot{\theta} = 0$ in equations 3(a) and 3(b) gives

$$C_D\left(\frac{3\rho_a}{4\rho_f D}\right)\dot{r}\sqrt{\dot{r}^2 + r^2\dot{\theta}^2} - r(\dot{\theta} + \omega)^2 = 0 \tag{4a}$$

$$C_D\left(\frac{3\rho_a}{4\rho_f D}\right)r\dot{\theta}\sqrt{\dot{r}^2 + r^2\dot{\theta}^2} + 2(\dot{\theta} + \omega)\dot{r} = 0 \tag{4b}$$

Division of equation (4a) by (4b) gives

$$2\dot{r}^2 = -r^2\dot{\theta}(\dot{\theta} + \omega) \tag{5}$$

Solving equation (5) for $\dot{r}$, and substituting into equation (4b) gives, after rearrangement and simplification

$$C_D\left(\frac{3\rho_a}{4\rho_f D}\right)r\dot{\theta}\sqrt{\dot{\theta}(\dot{\theta} - \omega)} = -2(\dot{\theta} + \omega)\sqrt{-\dot{\theta}(\dot{\theta} + \omega)}$$

Squaring both sides and rearranging gives

$$\dot{\theta} = -\frac{4(\dot{\theta} + \omega)^3}{C_D{}^2 r^2\left(\frac{3\rho_a}{4\rho_f D}\right)\dot{\theta}(\dot{\theta} - \omega)} \tag{6}$$

Equation (6) can be solved directly for the desired value of $\dot{\theta}$; however, the fact that C_D is also a function of $\dot{\theta}$ would make the computation quite laborious. Since the desired final value of $\dot{\theta}$ is small relative to ω, the equation can be simplified for computational purposes, without undue loss of accuracy, to

$$\dot{\theta} = \frac{4\omega^2}{C_D{}^2 r^2\left(\frac{3\rho_a}{4\rho_f D}\right)^2\dot{\theta}}$$

or

$$\dot{\theta} = -\frac{2\omega}{C_D r\left(\frac{3\rho_a}{4\rho_f D}\right)} \tag{7}$$

where the need for choosing the negative square root is apparent from equation (5). It must be remembered that C_D appearing in equation (7) is not a constant, but a function of the velocity (through the Reynolds number) and thus of $\dot{\theta}$.

The Reynolds number may be found from the equation

$$R = \frac{Dr}{\nu}\sqrt{\frac{\dot{\theta}(\dot{\theta} - \omega)}{2}}$$

where $r\sqrt{\frac{\dot{\theta}(\dot{\theta} - \omega)}{2}}$ is the total realtive velocity in terms of $\dot{\theta}$, (derived by substituting from equation (5) into the expression $\sqrt{\dot{r}^2 + r^2\dot{\theta}^2}$); and C_D may be found by referring to either figure 2 or equation (1), provided that R is in the valid range, $20 < R < 1000$, which appears to be the range of interest for the present problem. Equation (7) may be readily solved for the value of $\dot{\theta}$ by a simple iteration method (ref. 5). From the value of $\dot{\theta}$ thus derived, the value of $\dot{r}$ may then be obtained by use of equation (5); thus

$$\dot{r} = r\sqrt{\frac{\dot{\theta}(\dot{\theta} + \omega)}{-2}} \tag{8}$$

These values of $\dot{\theta}$ and $\dot{r}$ together with the radius will determine the final direction in the frame moving with the internal air. The final direction of the particle travel in the reference frame moving with the ram-jet unit is given by the angle

$$\tan^{-1}\frac{r(\dot{\theta} - \sigma)}{\dot{r}}$$

or

$$\tan^{-1}(\dot{\theta} - \sigma)\sqrt{\frac{-2}{\dot{\theta}(\dot{\theta} + \omega)}}$$

where the latter form does not require the intermediate calculation of $\dot{r}$. This method was checked for several cases against the paths calculated by the Bell computer. The inaccuracy was found to be small (about 3 percent) for the smallest particles ($D = 0.002$ in.) but to increase to about 15 percent for the largest particles ($D = 0.006$ in.). Thus, the method is probably satisfactorily accurate for the range of basic parameters, particularly particle size, of practical interest.

An approximate relation between the final radial velocity $\dot{r}$ and the centrifugal acceleration $\omega^2 r$ may be derived by substituting for $\dot{\theta}$ from equation (7) into equation (8). Equation (8) then becomes

$$\dot{r} = r\sqrt{\frac{\omega(\dot{\theta} + \omega)}{(C_D r)\left(\frac{3\rho_a}{4\rho_f D}\right)}}$$

from which, since $\dot{\theta}$ is small relative to ω, it is apparent that

$$\dot{r} \propto \sqrt{\omega^2 r}$$

That is, the final radial velocity is approximately proportional to the square root of the centrifugal acceleration.

CONCLUDING REMARKS

Simultaneous differential equations, amenable to numerical integration, have been developed for the fuel-spray-particle paths in a ram-jet engine operating on the tip of a helicopter rotor blade. A method of determining the approximate asymptotic direction of the motion has also been given; that is, a method of finding the approximate outward deviation of the path in the combustion chamber.

Solutions of the equations for a range of conditions show that the centrifugal effect tends to throw the heavier fuel particles to the outer wall of the ram-jet unit, while particles fine enough to minimize this effect may not reach far enough laterally from the nozzle to provide a favorable fuel distribution in the combustion chamber. Several methods of overcoming the problem are suggested, such as using a distribution of fine-spray nozzles and skewing the combustion chamber outward.

Langley Aeronautical Laboratory,
National Advisory Committee for Aeronautics,
Langley Field, Va.

REFERENCES

1. Eisner, F.: Das Widerstandsproblem. Vol. I of Proc. 3rd Int. Cong. Appl. Mech., (Stockholm, Aug. 24-29, 1930), P.A. Norstedt & Soner, 1931, pp. 23-41, Diskussion, pp. 41-42.

2. Castleman, R. A.: The Resistance to the Steady Motion of Small Spheres in Fluids. NACA TN 231, 1926.

3. Fluid Motion Panel of the Aeronautical Research Committee and Others: (S. Goldstein, ed.): Modern Developments in Fluid Dynamics. Vol. II, The Clarendon Press (Oxford), 1938, p. 493.

4. Levy, H., and Baggott, E. A.: Numerical Solutions of Differential Equations. First American ed., Dover Publications (New York), 1950, ch. III.

5. Uspensky, J. V.: Theory of Equations. McGraw-Hill Book Company (New York), 1948, ch. VIII.

TABLE I.- TABLE OF PARAMETERS AND INITIAL VALUES FOR CASES CALCULATED

Particle diameter, D, in.	Rotor radius, r_o, ft	Rotor tip speed, fps	Internal-flow velocity relative to nozzle, fps	Fuel injection velocity relative to nozzle, fps	Fuel injection angle, β, deg
[a]0.002, 0.004, 0.006	15, 25	800,1000	200	150	-45, 0, 45
.004	15	1000	200	250	-45, 0, 45
.002	15	1000	200	250	0
.006	15	1000	200	250	0
.004	25	800	200	250	-45, 45
.004	25	1000	200	250	-45, 45
.004	15	1000	400	150	-45, 0, 45
.002	15	1000	400	150	0
.006	15	1000	400	150	0
.004	25	800	400	150	-45, 45
.004	25	1000	400	150	-45, 45
.004	15	1000	400	250	-45, 0, 45
.002	15	1000	400	250	0
.006	15	1000	400	250	0
.004	25	800	400	250	-45, 45
.004	25	1000	400	250	-45, 45

[a]Calculations were made for all possible combinations of the values in this line (36 cases).

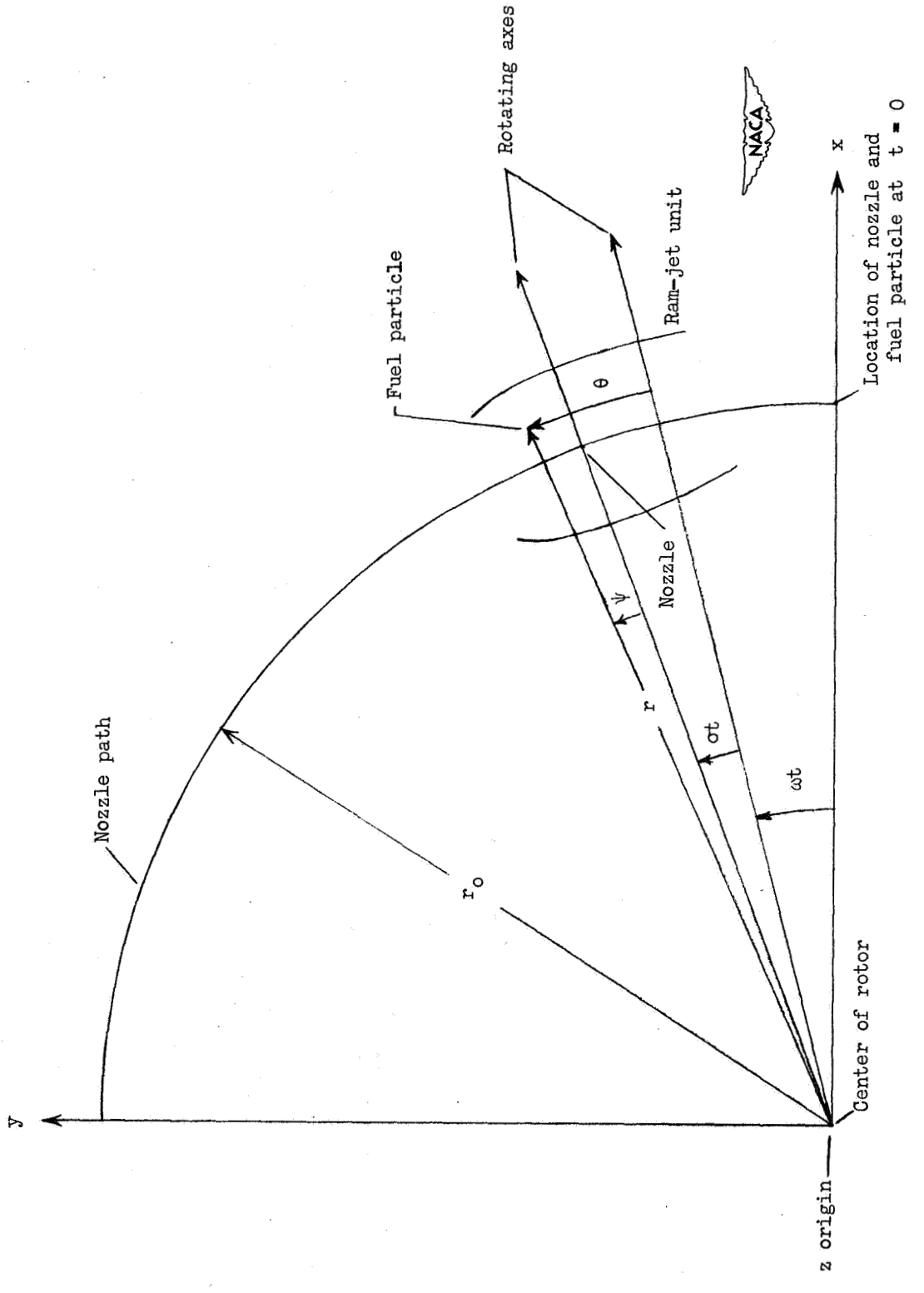

Figure 1.- Sketch of the relationship between the three coordinate systems. The z-axis is normal to plane of paper.

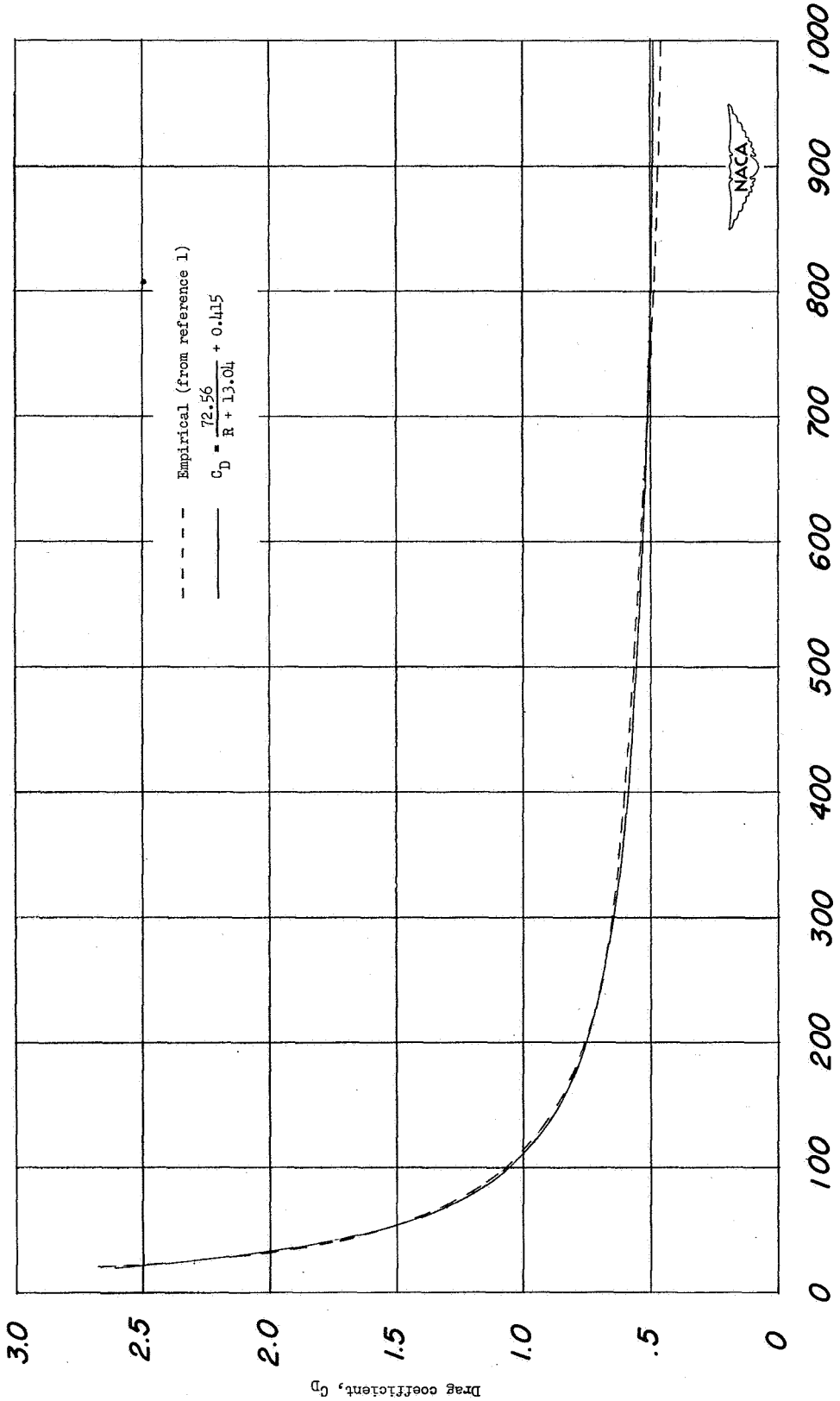

Figure 2.- Experimental sphere-drag coefficient against Reynolds numbers, and comparison curve for algebraic expression used in calculations.

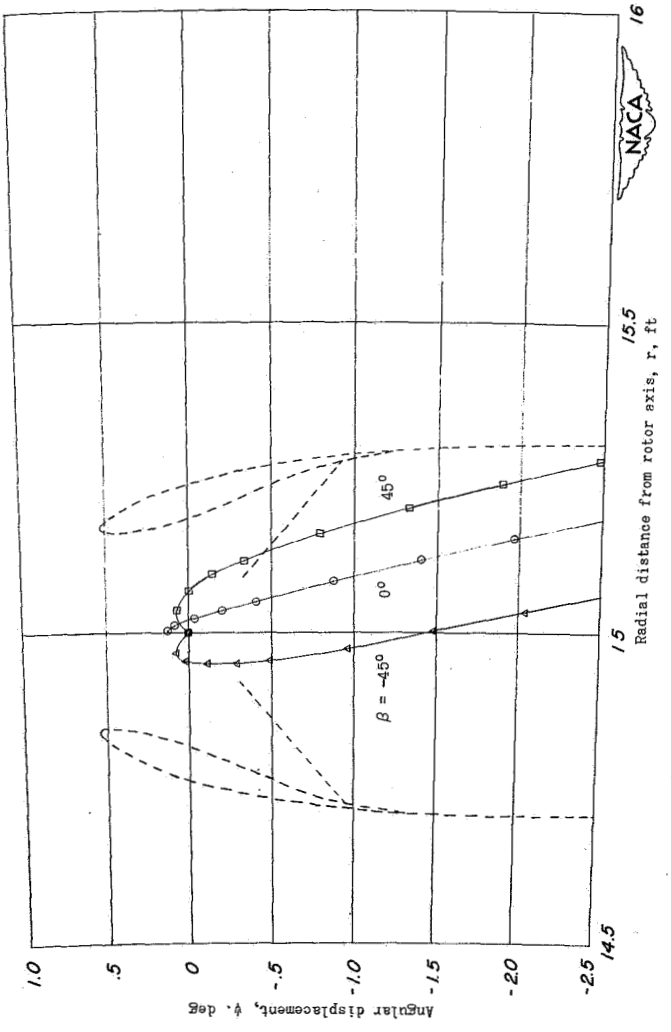

(a) Particle diameter, D, 0.002 inch.

Figure 3.- Paths of fuel particles ejected in plane of rotor, with $\beta = -45°$, 0°, and 45°. Rotor radius (to nozzle), 15 feet; tip speed, 800 fps; internal air speed relative to nozzle, 200 fps; fuel-injection velocity relative to nozzle, 150 fps; centrifugal acceleration at nozzle, 1330g.

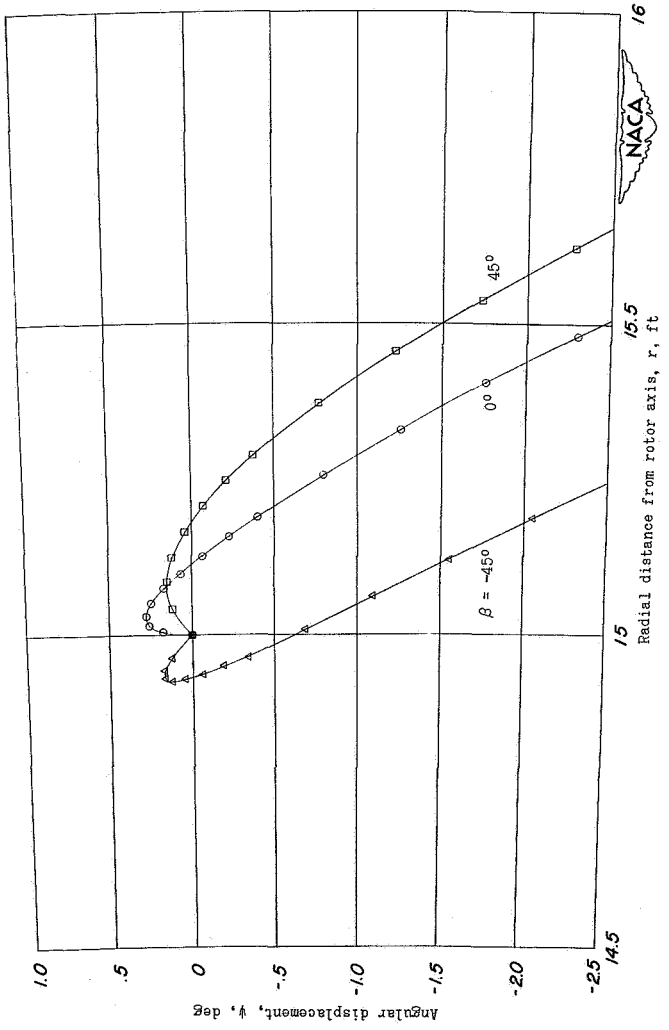

(b) Particle diameter, D, 0.004 inch.

Figure 3.- Continued.

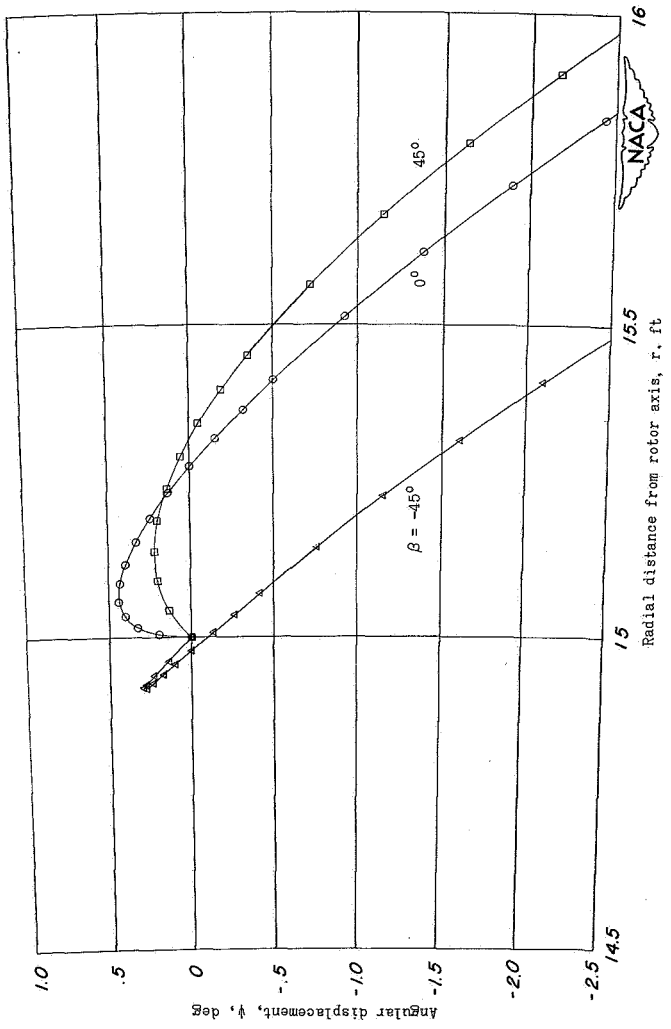

(c) Particle diameter, D, 0.006 inch.

Figure 3.- Concluded.

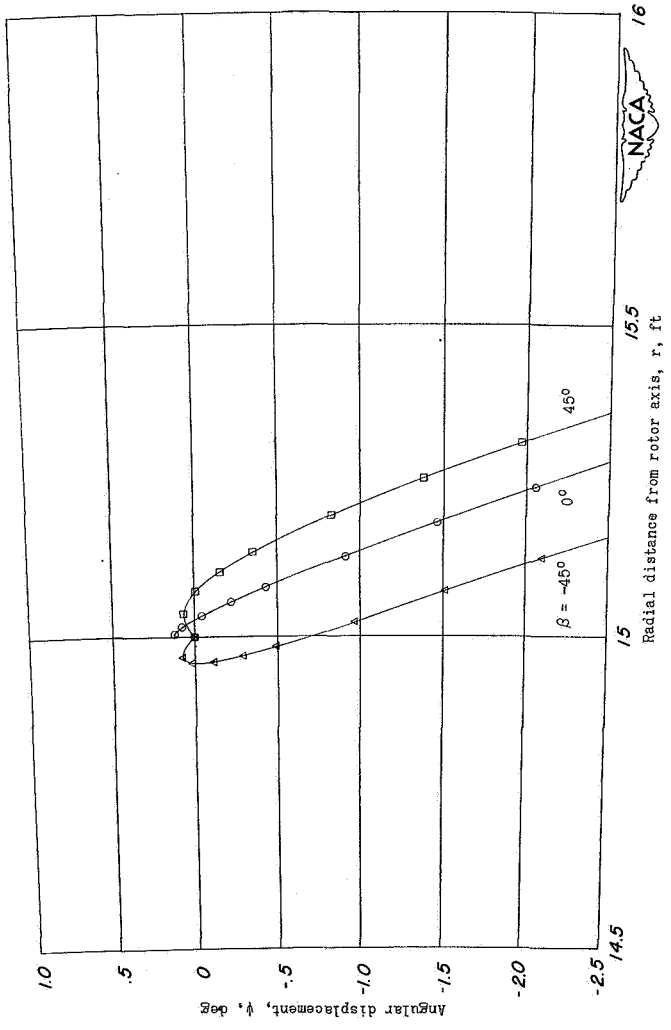

(a) Particle diameter, D, 0.002 inch.

Figure 4.- Paths of fuel particles ejected in plane of rotor, with $\beta = -45°$, 0°, and 45°. Rotor radius (to nozzle), 15 feet; tip speed, 1000 fps; internal air speed relative to nozzle, 200 fps; fuel-injection velocity relative to nozzle, 150 fps; centrifugal acceleration at nozzle, 2070g.

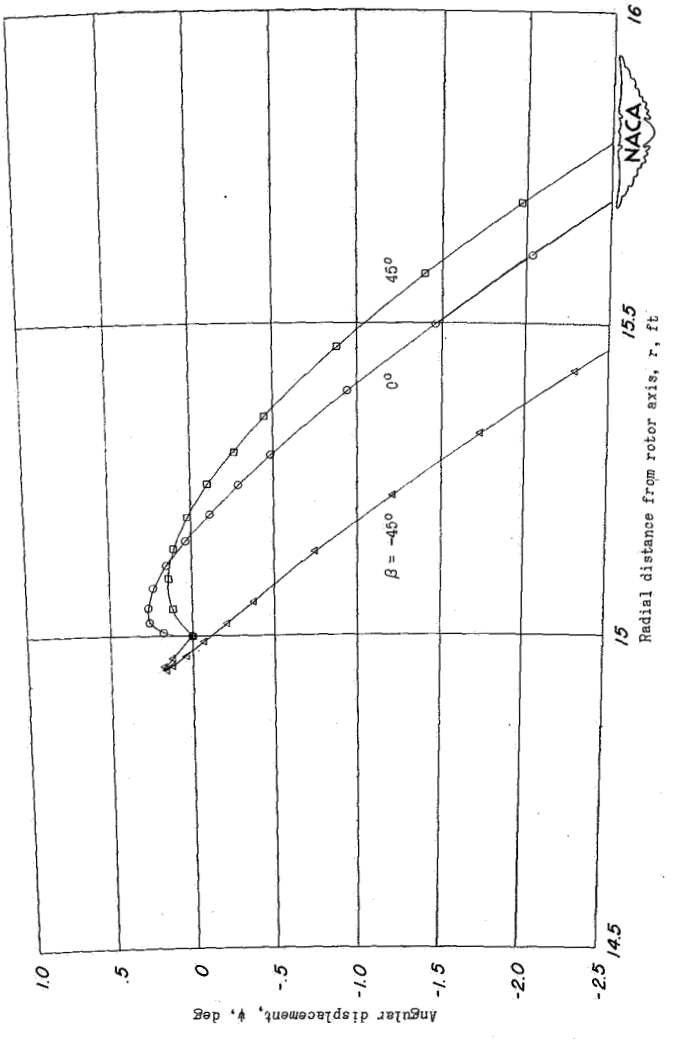

(b) Particle diameter, D, 0.004 inch.

Figure 4.- Continued.

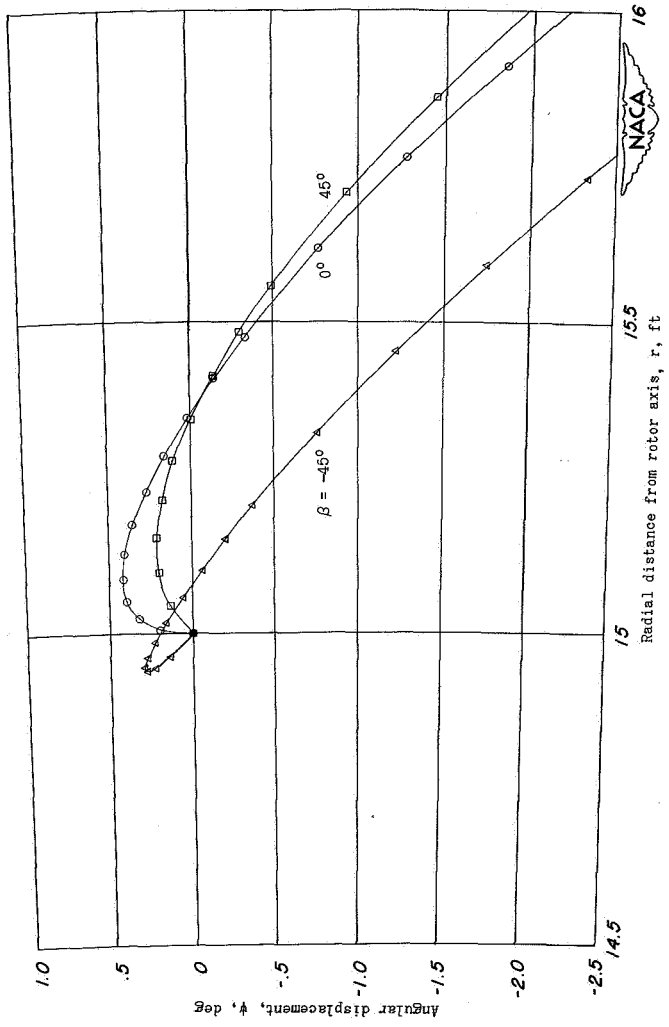

(c) Particle diameter, D, 0.006 inch.

Figure 4.- Concluded.

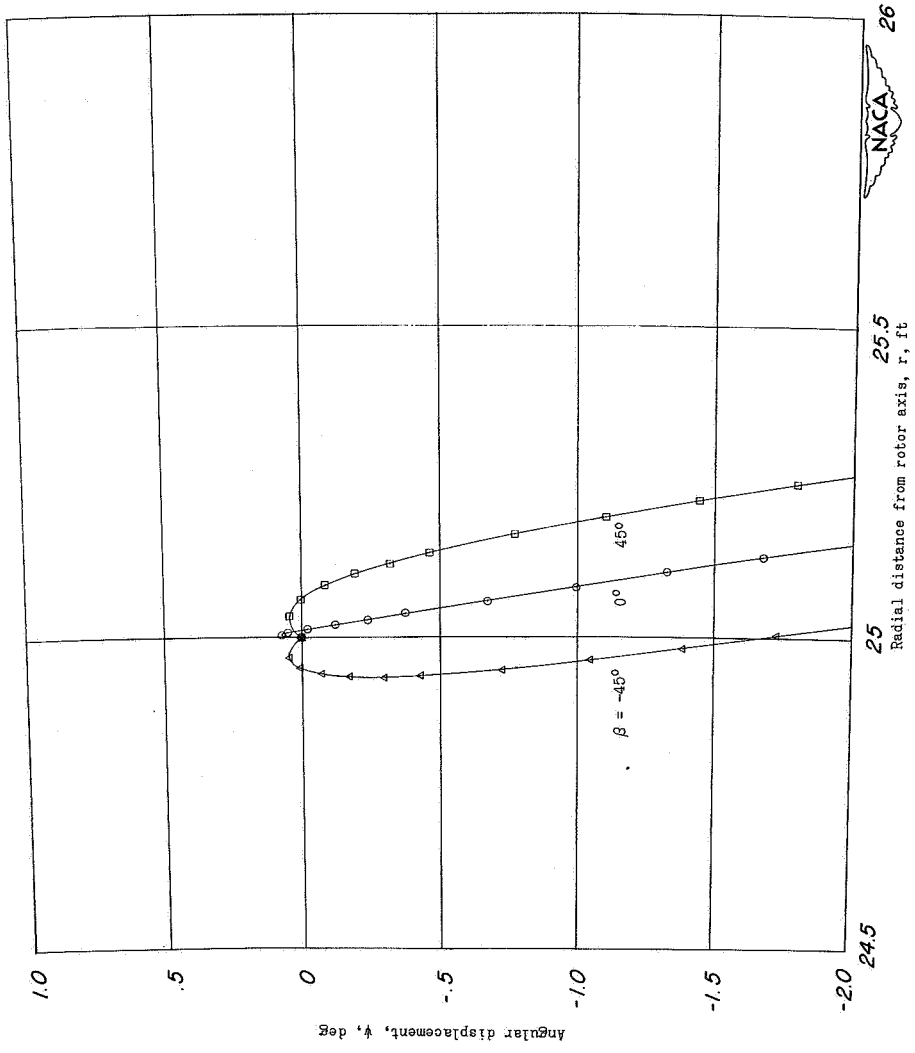

(a) Particle diameter, D, 0.002 inch.

Figure 5.- Paths of fuel particles ejected in plane of rotor, with $\beta = -45^\circ$, 0°, and 45°. Rotor radius (to nozzle), 25 feet; tip speed, 800 fps; internal air speed relative to nozzle, 200 fps; fuel-injection velocity relative to nozzle, 150 fps; centrifugal acceleration at nozzle, 795g.

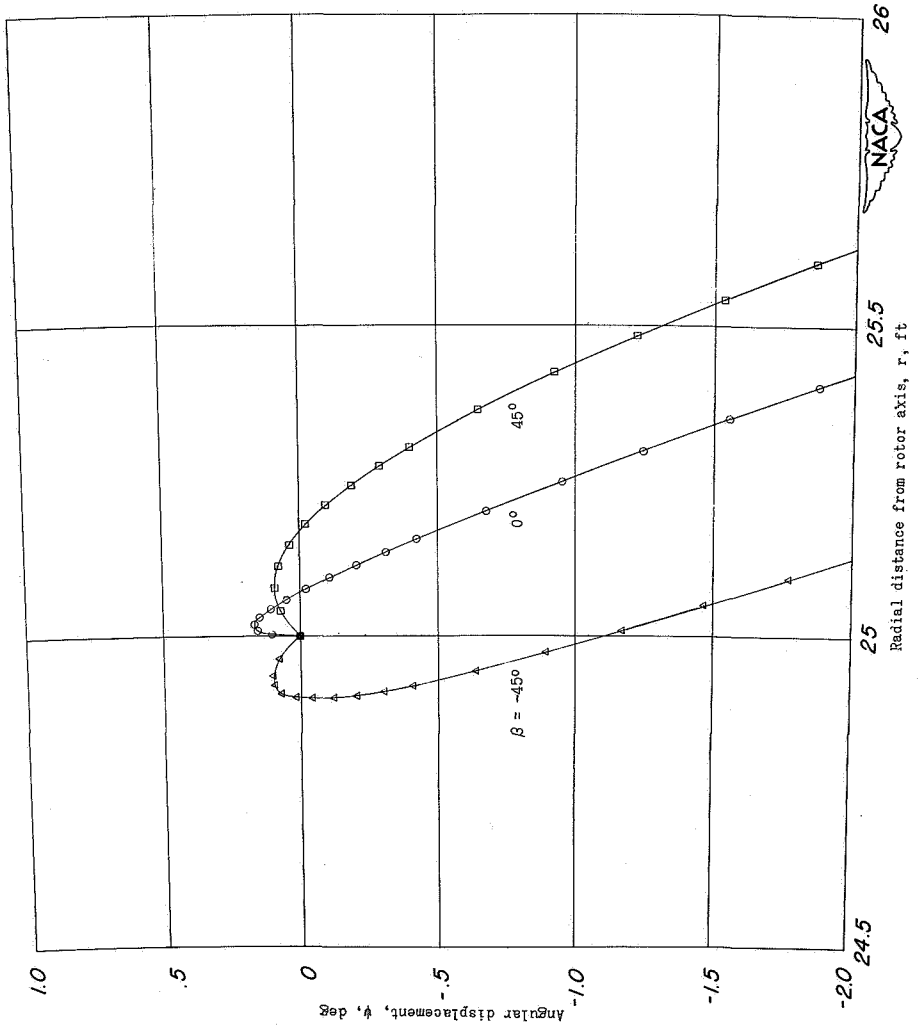

(b) Particle diameter, D, 0.004 inch.

Figure 5.- Continued.

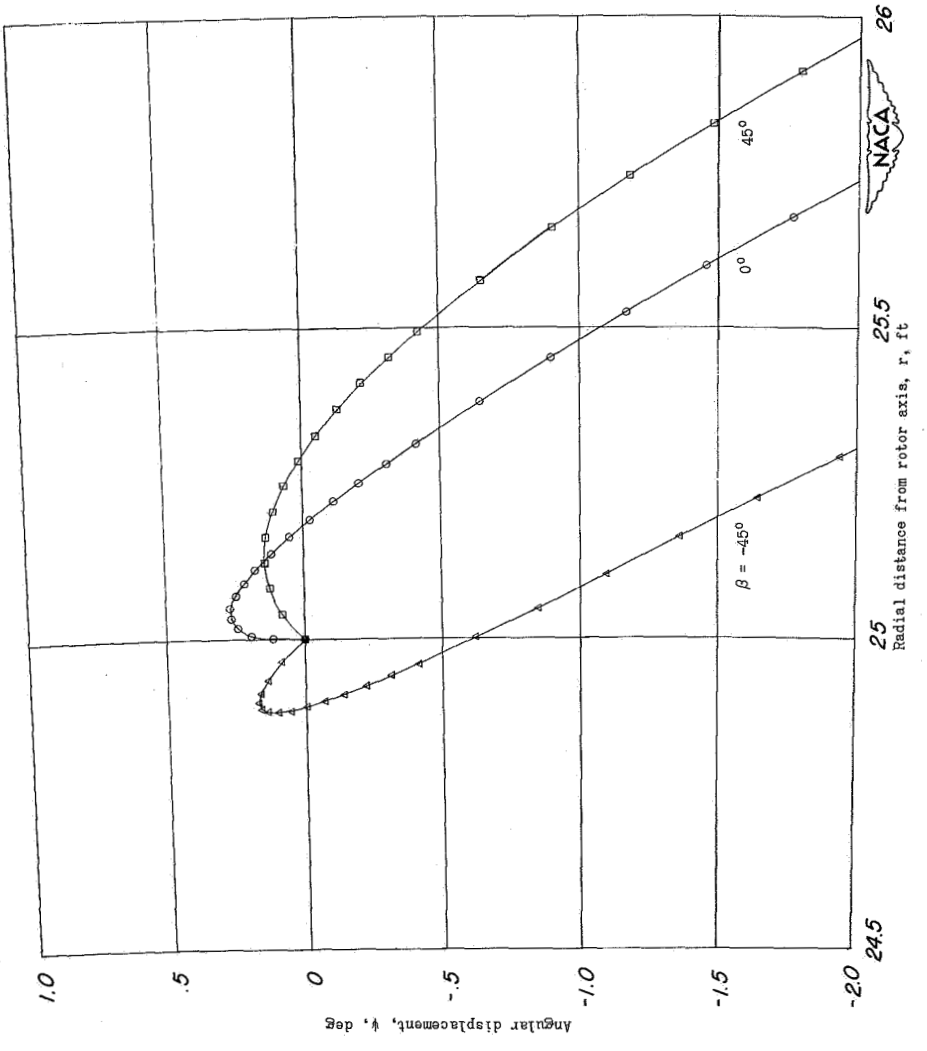

(c) Particle diameter, D, 0.006 inch.

Figure 5.- Concluded.

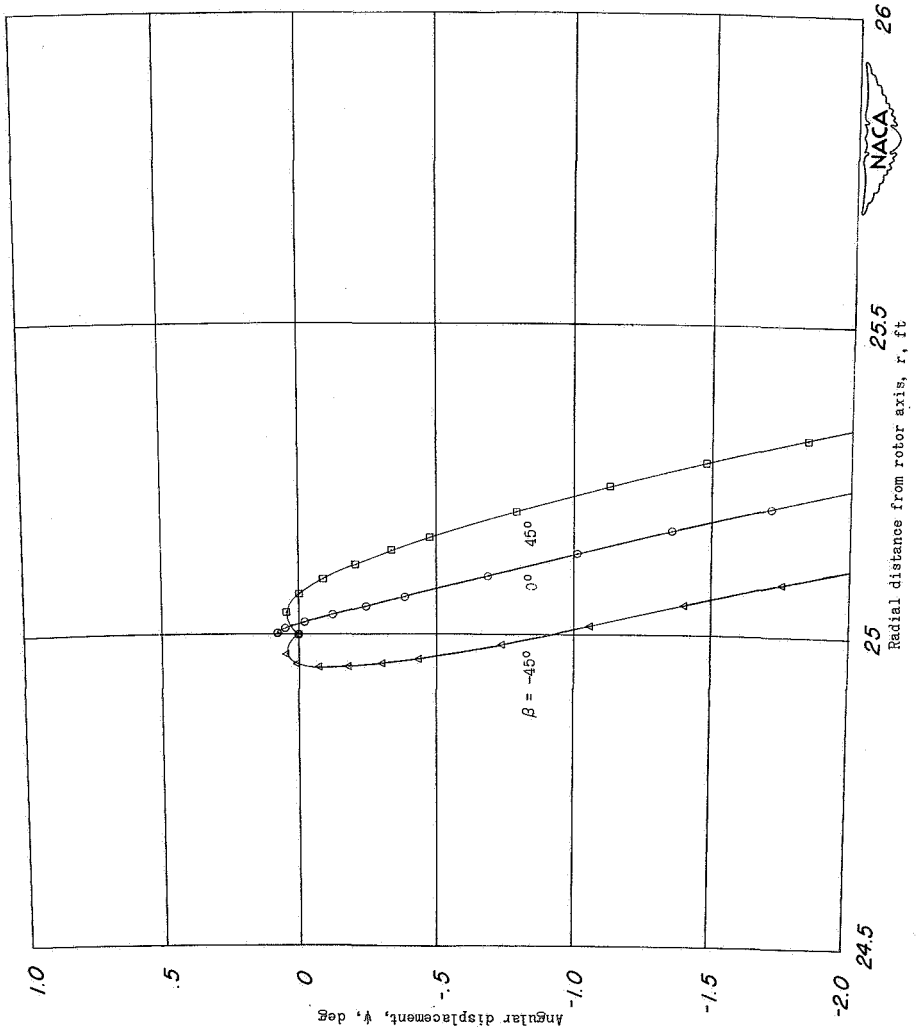

(a) Particle diameter, D, 0.002 inch.

Figure 6.- Paths of fuel particles ejected in plane of rotor, with $\beta = -45°$, $0°$, and $45°$. Rotor radius (to nozzle), 25 feet; tip speed, 1000 fps; internal air speed relative to nozzle, 200 fps; fuel-injection velocity relative to nozzle, 150 fps; centrifugal acceleration at nozzle, 1240g.

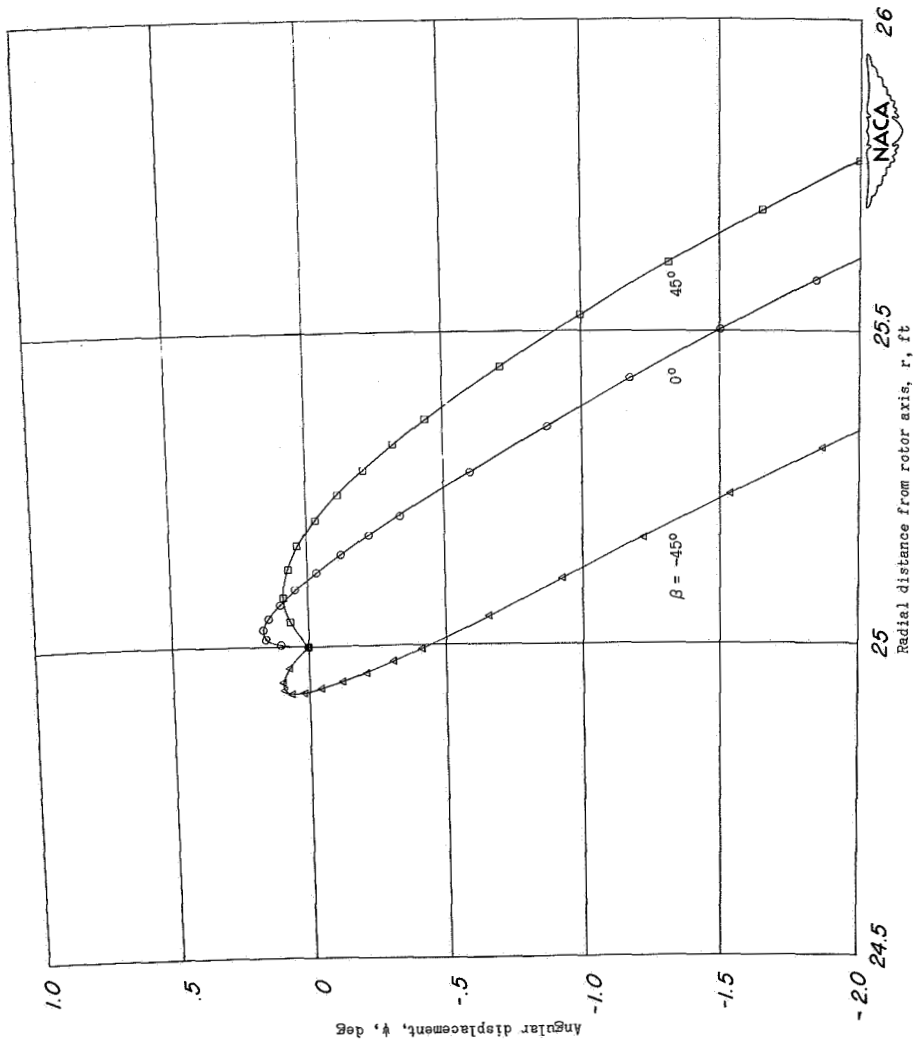

(b) Particle diameter, D, 0.004 inch.

Figure 6.- Continued.

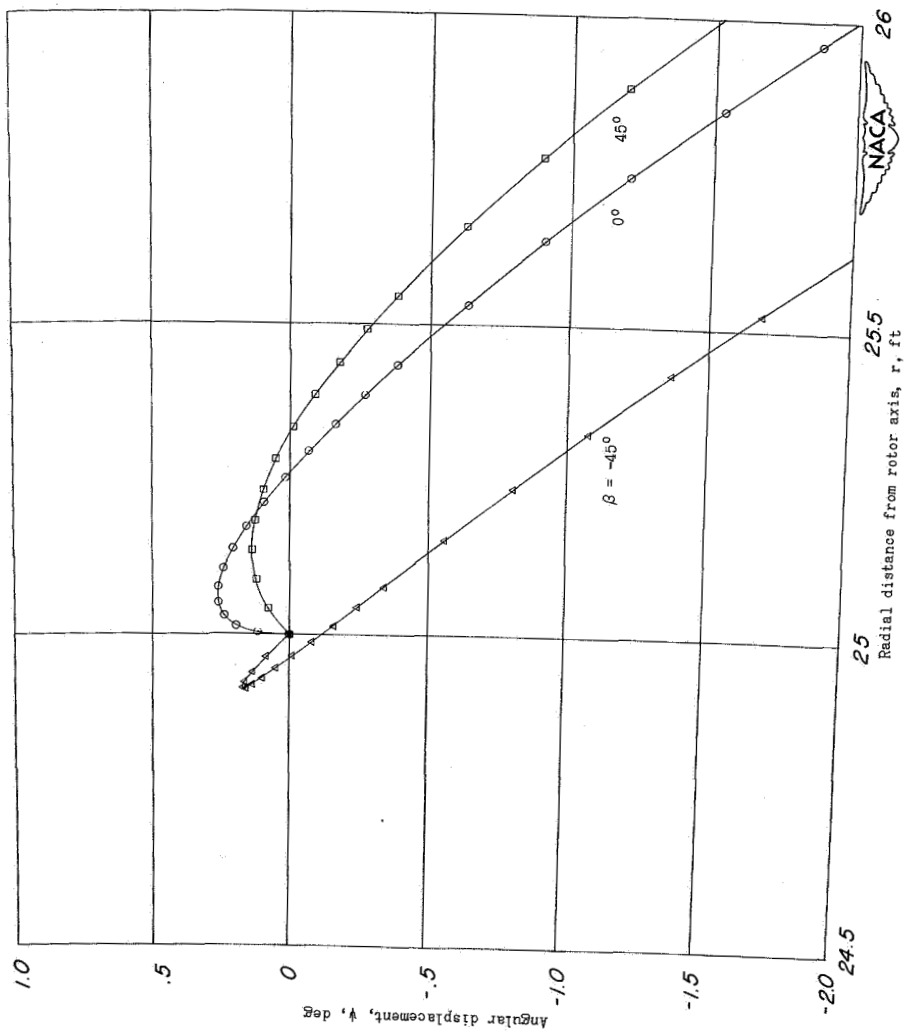

(c) Particle diameter, D, 0.006 inch.

Figure 6.- Concluded.

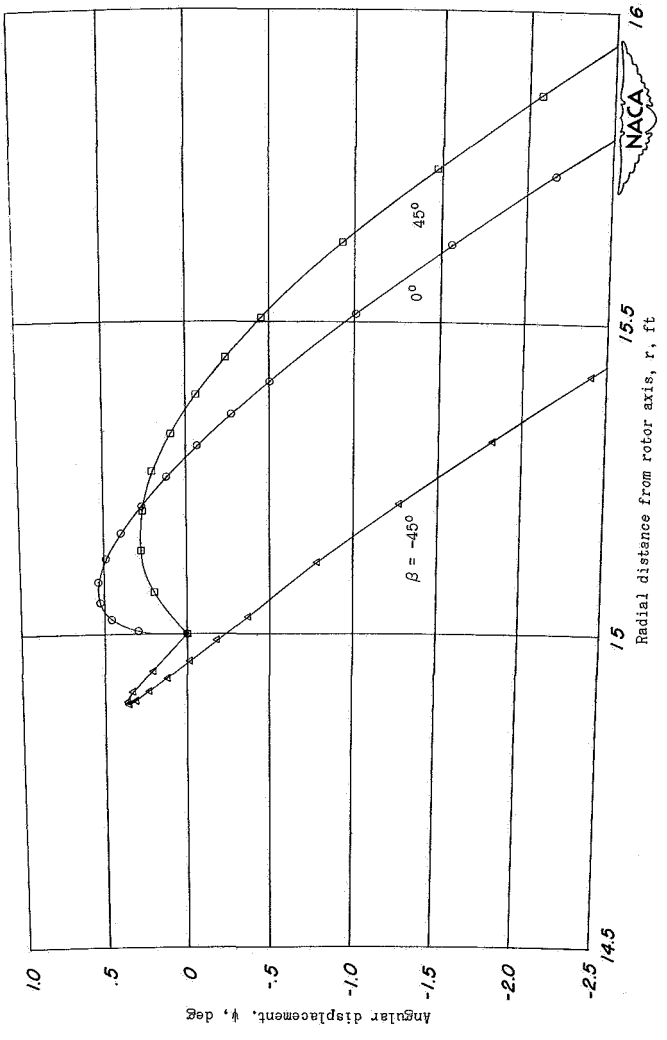

Figure 7.- Paths of 0.004-inch-diameter fuel particles ejected in plane of of rotor, with $\beta = -45^\circ$, 0°, and 45°. Rotor radius (to nozzle), 15 feet; tip speed, 1000 fps; internal air speed relative to nozzle, 200 fps; fuel-injection velocity relative to nozzle, 250 fps; centrifugal acceleration at nozzle, 2070g.

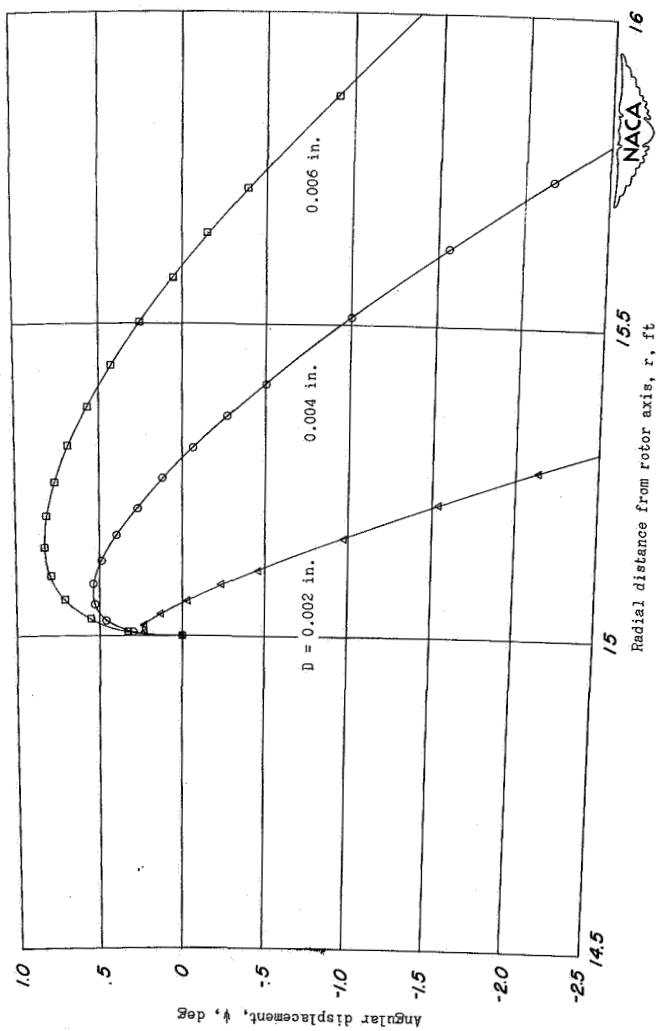

Figure 8.- Paths of 0.002-, 0.004-, and 0.006-inch diameter fuel particles ejected in plane of rotor, with $\beta = 0^{\circ}$. Rotor radius (to nozzle), 15 feet; tip speed, 1000 fps; internal air speed relative to nozzle, 200 fps; fuel-injection velocity relative to nozzle, 250 fps; centrifugal acceleration at nozzle, 2070g.

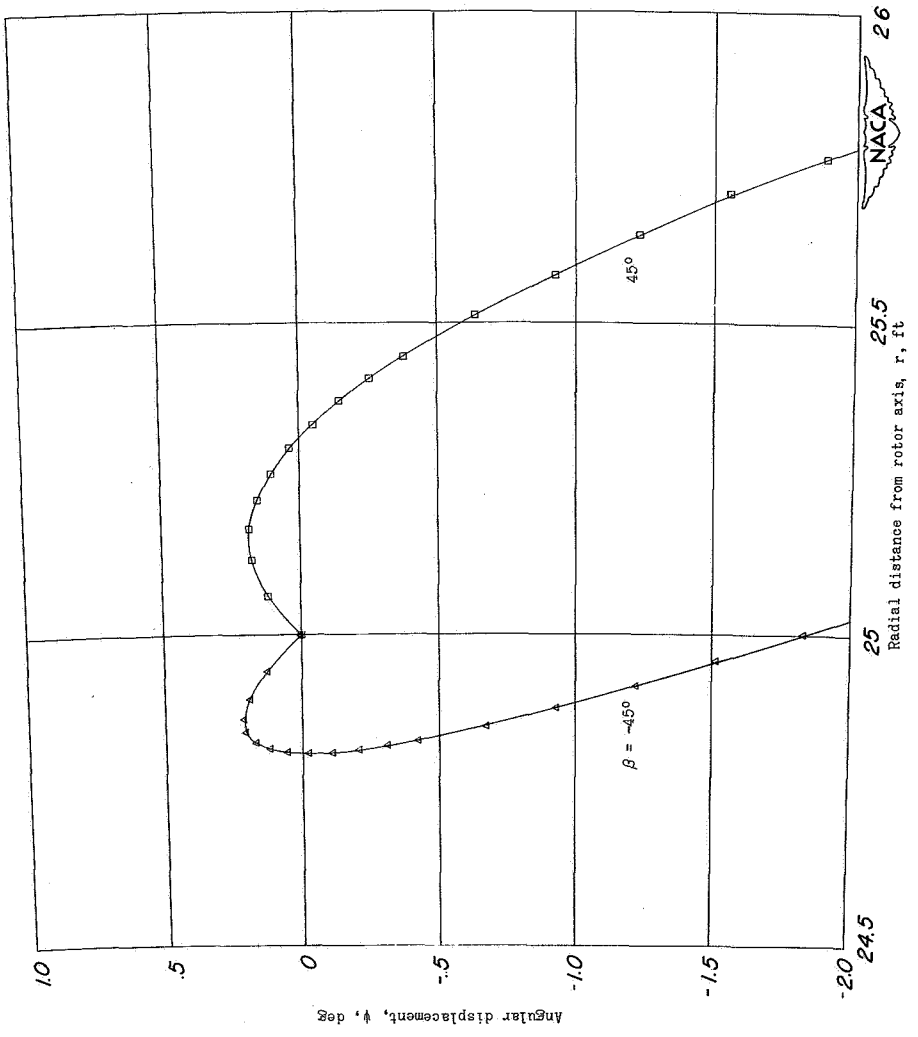

Figure 9.- Paths of 0.004-inch-diameter fuel particles ejected in plane of rotor, with $\beta = -45°$ and 45°. Rotor radius (to nozzle), 25 feet; tip speed, 800 fps; internal air speed relative to nozzle, 200 fps; fuel-injection velocity relative to nozzle, 250 fps; centrifugal acceleration at nozzle, 795g.

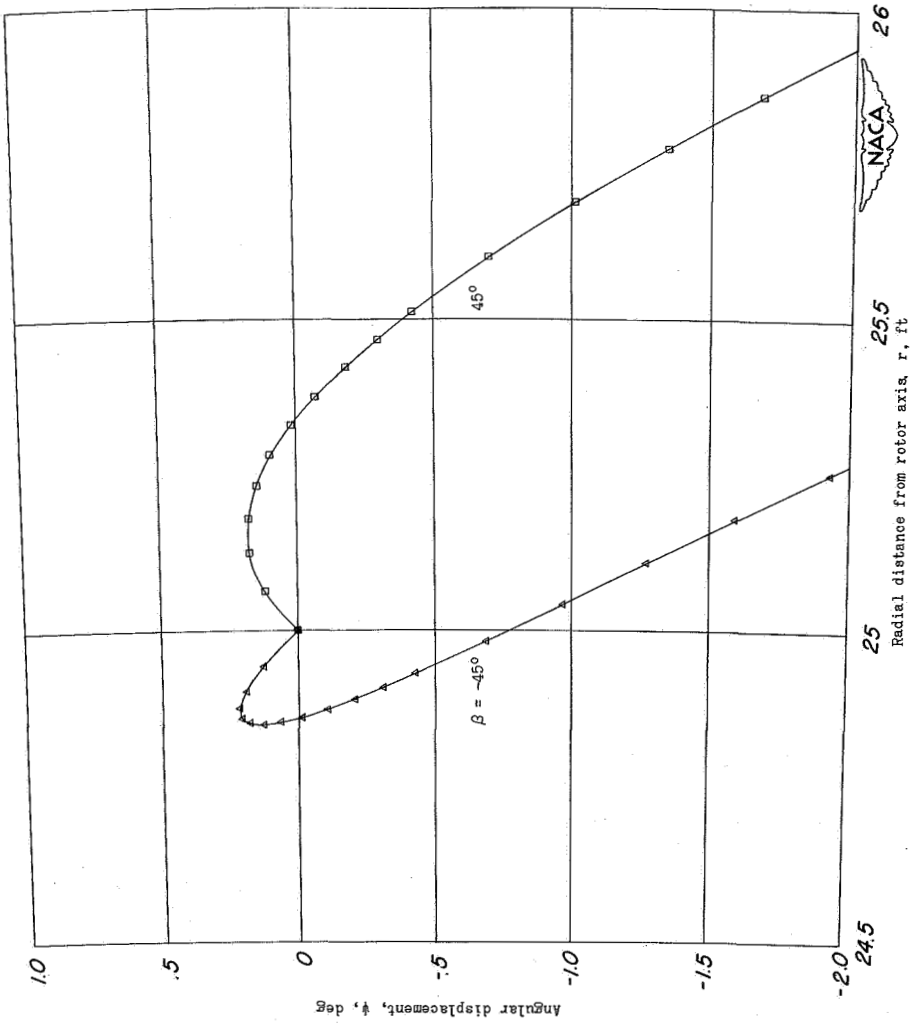

Figure 10.- Paths of 0.004-inch-diameter fuel particles ejected in plane of rotor, with $\beta = -45^\circ$ and 45°. Rotor radius (to nozzle), 25 feet; tip speed, 1000 fps; internal air speed relative to nozzle, 200 fps; fuel-injection velocity relative to nozzle, 250 fps; centrifugal acceleration at nozzle, 1240g.

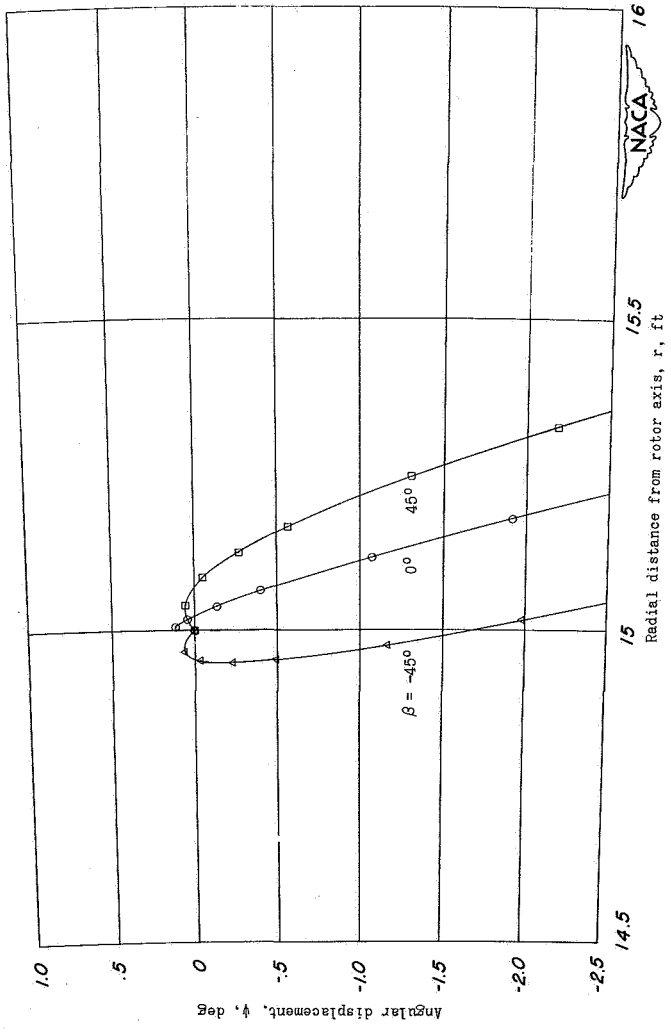

Figure 11.- Paths of 0.004-inch-diameter fuel particles ejected in plane of rotor, with β = -45°, 0°, and 45°. Rotor radius (to nozzle), 15 feet; tip speed, 100 fps; internal air speed relative to nozzle, 400 fps; fuel-injection velocity relative to nozzle, 150 fps; centrifugal acceleration at nozzle, 207g.

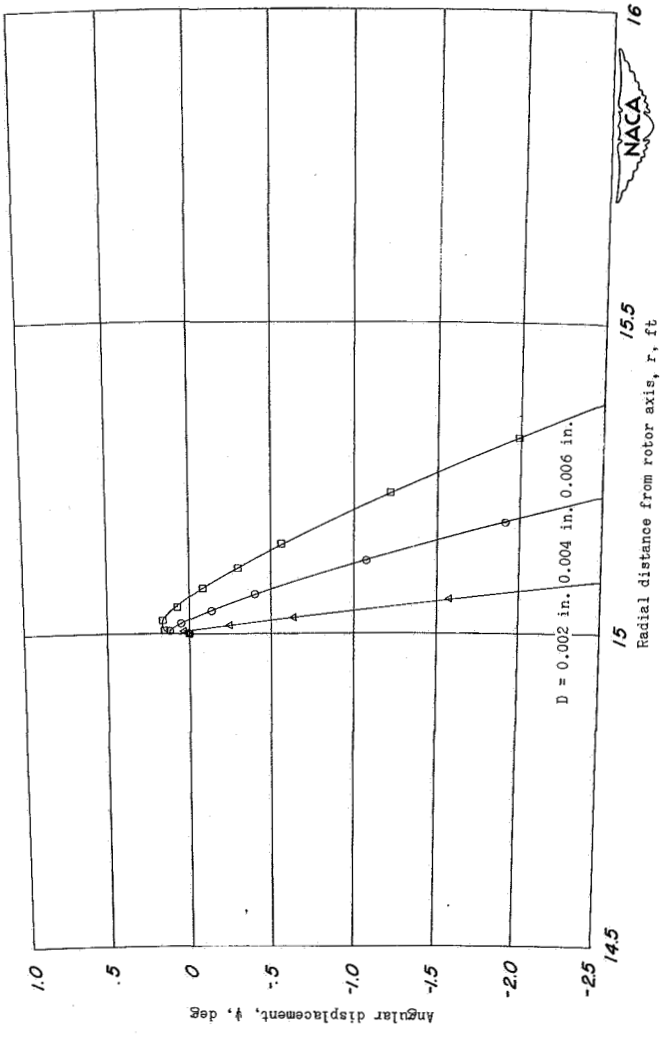

Figure 12.- Paths of 0.002-, 0.004-, and 0.006-inch-diameter fuel particles ejected in plane of rotor, with $\beta = 0^{\circ}$. Rotor radius (to nozzle), 15 feet; tip speed, 1000 fps, internal air speed relative to nozzle, 400 fps; fuel-injection velocity relative to nozzle, 150 fps; centrifugal acceleration at nozzle, 2070g.

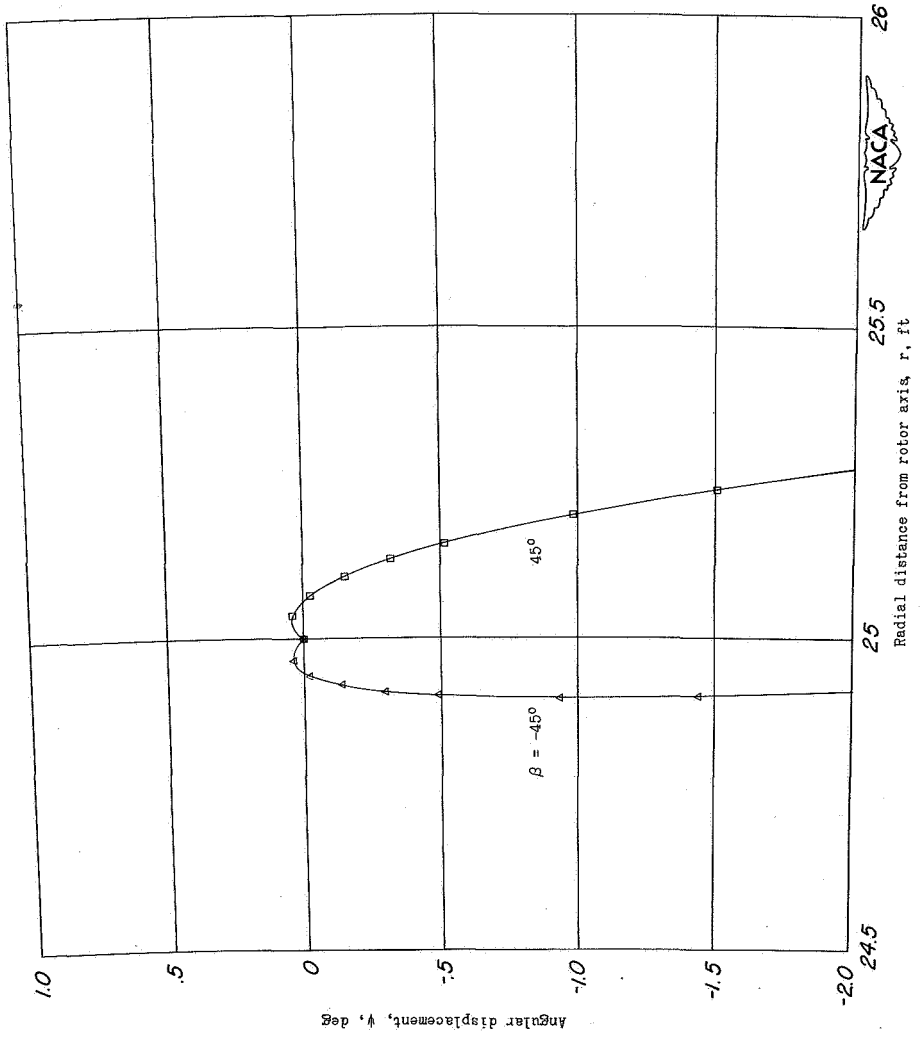

Figure 13.- Paths of 0.004-inch-diameter fuel particles ejected in plane of rotor, with $\beta = -45^\circ$ and 45°. Rotor radius (to nozzle), 25 feet; tip speed, 800 fps; internal air speed relative to nozzle, 400 fps; fuel-injection velocity relative to nozzle, 150 fps; centrifugal acceleration at nozzle, 795g.

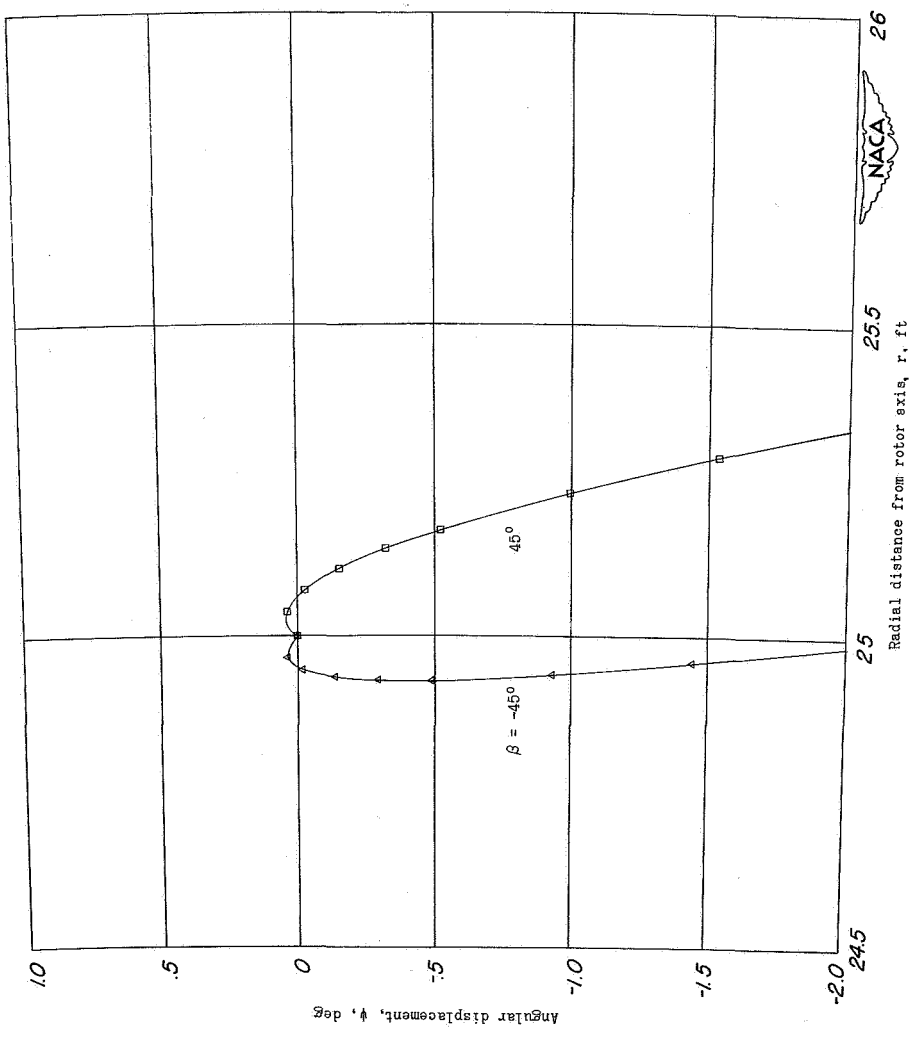

Figure 14.- Paths of 0.004-inch-diameter fuel particles ejected in plane of rotor, with $\beta = -45°$ and 45°. Rotor radius (to nozzle), 25 feet; tip speed, 1000 fps; internal air speed relative to nozzle, 400 fps; fuel-injection velocity relative to nozzle, 150 fps; centrifugal acceleration at nozzle, 1240g.

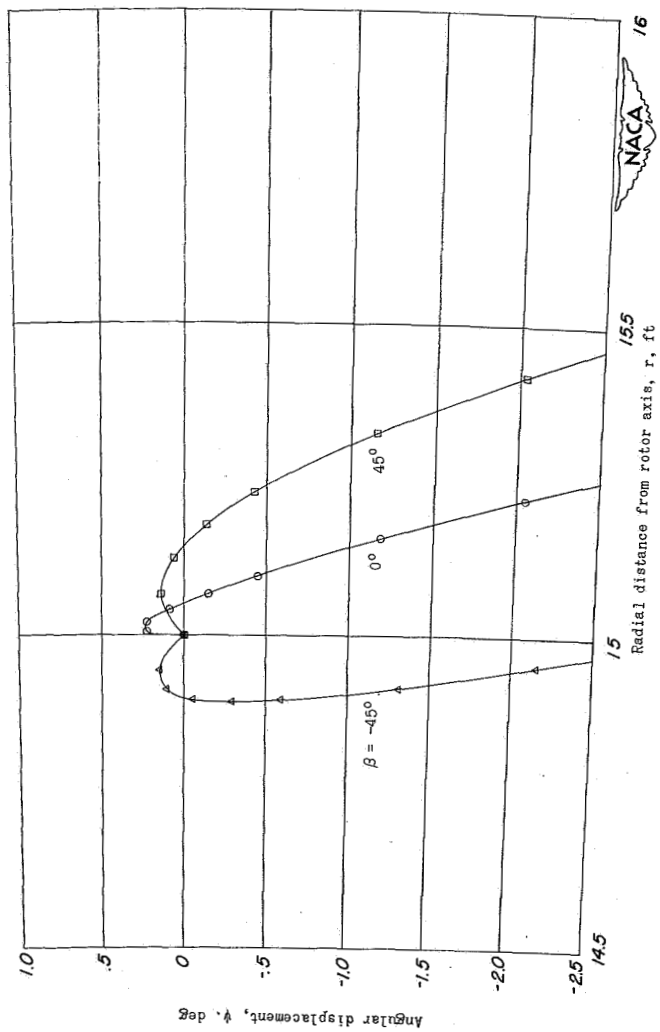

Figure 15.- Paths of 0.004-inch-diameter fuel particles ejected in plane of rotor, with $\beta = -45^{\circ}$, 0°, and 45°. Rotor radius (to nozzle), 15 feet; tip speed, 1000 fps; internal air speed relative to nozzle; 400 fps; fuel-injection velocity relative to nozzle, 250 fps; centrifugal acceleration at nozzle, 2070g.

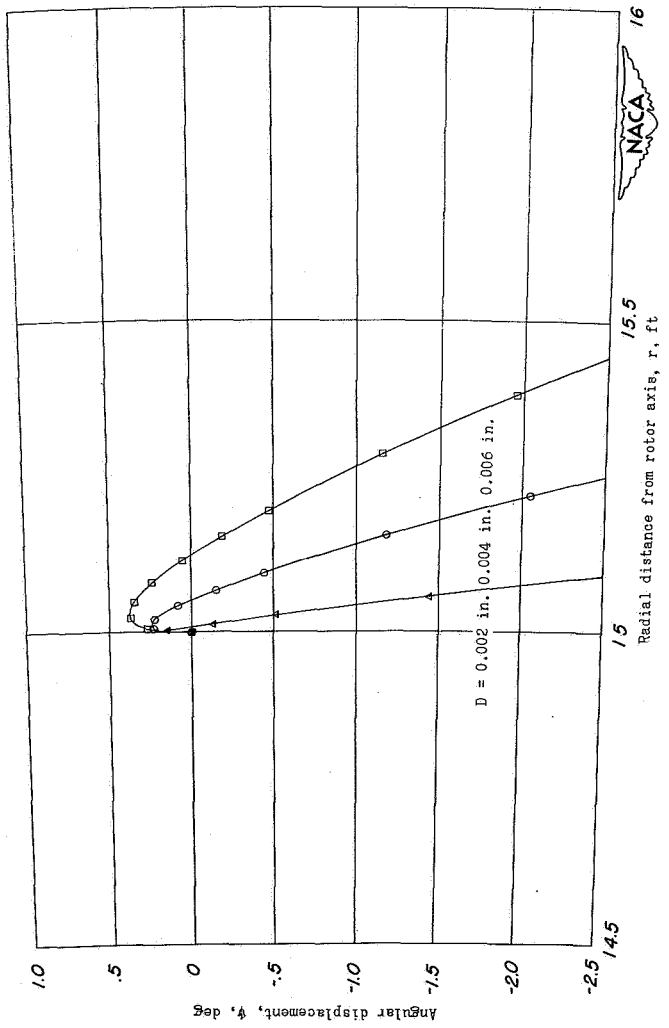

Figure 16.- Paths of 0.002-, 0.004-, and 0.006-inch-diameter fuel particles ejected in plane of rotor, with $\beta = 0^{\circ}$. Rotor radius (to nozzle), 15 feet; tip speed, 1000 fps; internal air speed relative to nozzle, 400 fps, fuel-injection velocity relative to nozzle, 250 fps; centrifugal acceleration at nozzle, 2070g.

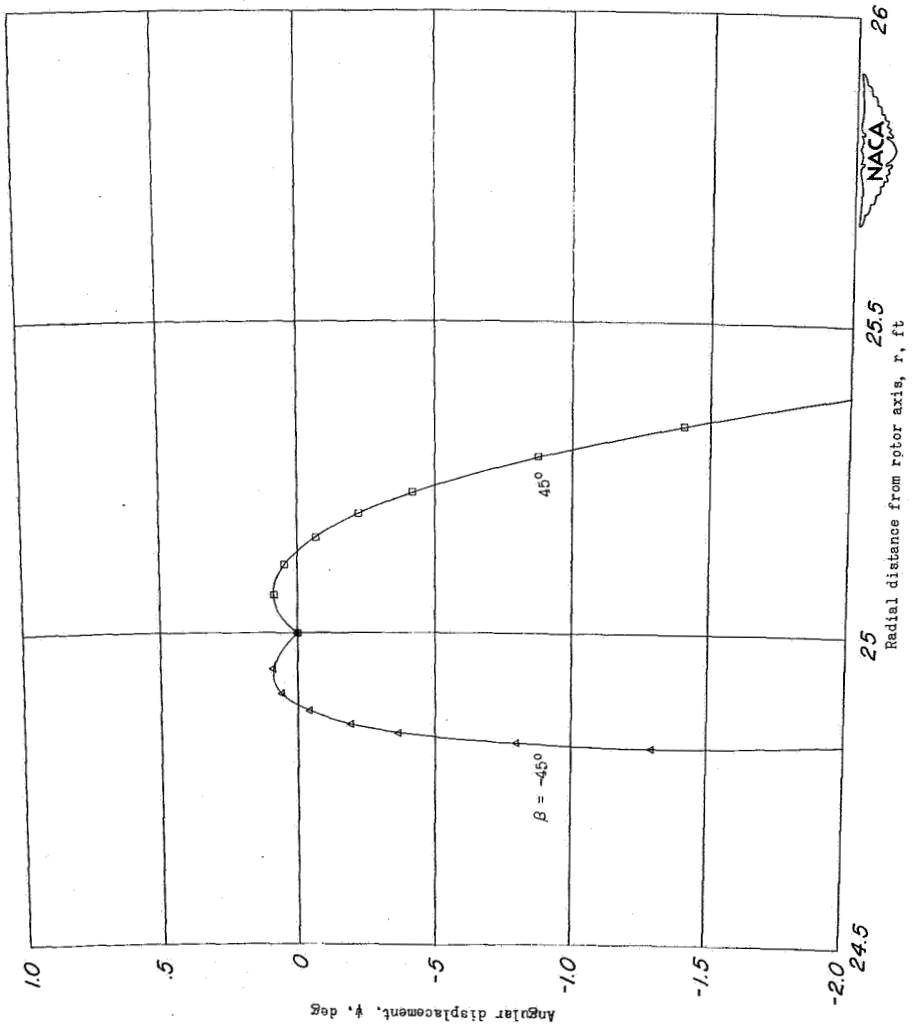

Figure 17.- Paths of 0.004-inch-diameter fuel particles ejected in plane of rotor, with $\beta = -45^{\circ}$ and 45°. Rotor radius (to nozzle), 25 feet; tip speed, 800 fps; internal air speed relative to nozzle, 400 fps; fuel-injection velocity relative to nozzle, 250 fps; centrifugal acceleration at nozzle, 795g.

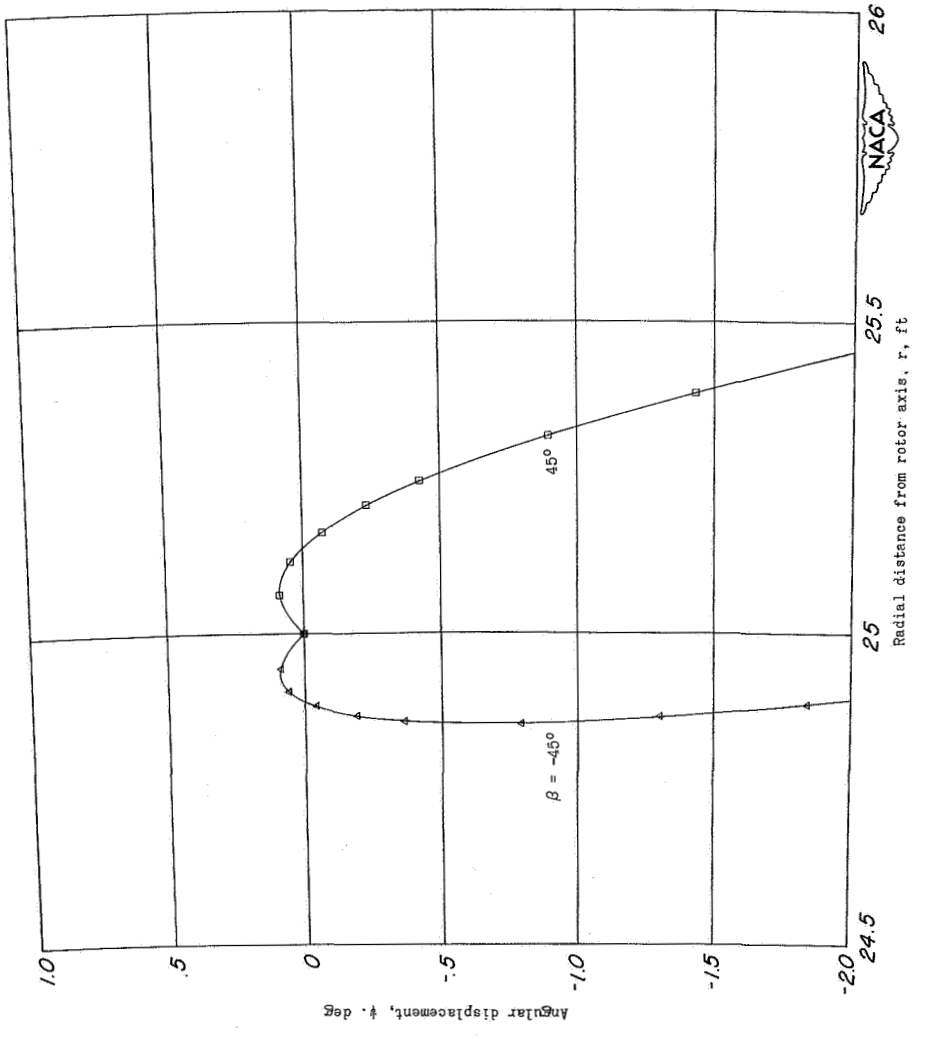

Figure 18.- Paths of 0.004-inch-diameter fuel particles ejected in plane of rotor, with $\beta = -45^{\circ}$ and 45°. Rotor radius (to nozzle), 25 feet; tip speed, 1000 fps; internal air speed relative to nozzle, 400 fps; fuel-injection velocity relative to nozzle, 250 fps; centrifugal acceleration at nozzle, 1240g.

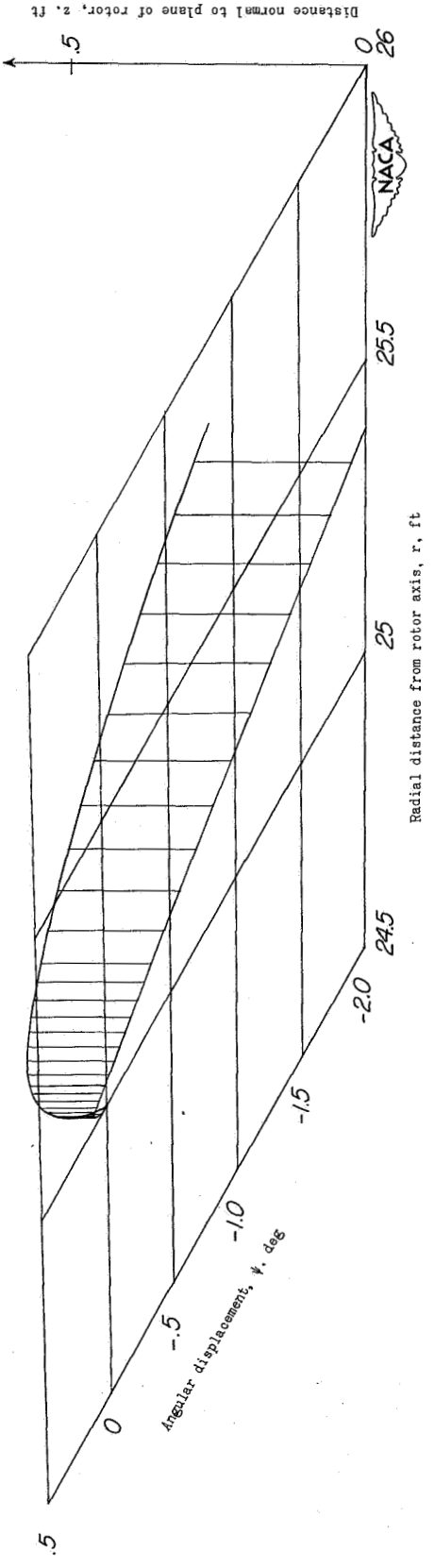

Figure 19.- Path of 0.004-inch-diameter fuel particle ejected at an angle of 45° out of the plane of the rotor, with $\beta = 0$. Rotor radius (to nozzle), 25 feet; tip speed, 800 fps; internal air speed relative to nozzle, 200 fps; fuel-injection velocity relative to nozzle, 150 fps; centrifugal acceleration at nozzle, 795g.